

Finite Element Based Cross-Sectional Buckling Optimization for a Constant Area, Pinned-Pinned Composite Column

Presented to the Academic Faculty
The University of Texas at Arlington

by

Anirudh Srinivas

In Partial Fulfillment of
the Requirements for the Degree
Master of Science in Mechanical Engineering

Department of Mechanical and Aerospace Engineering
The University of Texas at Arlington
Arlington, TX 76019

May 2016

Copyright © by Anirudh Srinivas 2016

All Rights Reserved



Acknowledgements

I would like to express my sincere gratitude to my supervising professor, Dr. D. S. Dancila, for his support and guidance.

I would also like to thank Dr. Wen S. Chan and Dr. Kent L. Lawrence for serving on my thesis committee.

I would like to especially thank my parents T. N. Srinivas and P. Mahalakshmi for their support and encouragement.

Last but not the least, I would like to thank God Almighty for giving me this opportunity.

I would like to dedicate this work to my parents T. N. Srinivas and P. Mahalakshmi.

Abstract

Finite Element Based Cross-Sectional Buckling Optimization for a Constant Area, Pinned-Pinned Composite Column

Supervising Professor: Dr. D. Stefan Dancila

In archery, dynamic buckling compromises the target accuracy of arrows. For both dynamic and quasi-static buckling, the buckling load depends on the cross-sectional area moment of inertia, which can be increased by modifying the cross-sectional shape of the arrow shaft. Arrows commercially available today are made up of composite materials and have a tubular circular cross-section. In this study an effort has been made to optimize the cross-sectional shape of the composite arrow shaft, using finite element based, quasi-static buckling analysis keeping the length and area of the cross-section constant. The composite column is pinned at both ends and is assumed to be made up of ten plies with fibers oriented along the length of the column. Four cross-sectional shapes: tubular circular, tubular equilateral triangular, star shaped and star with beads are analyzed in this study. The composite column is modeled in ABAQUS, and the buckling load is determined by using the “Linear Perturbation, Buckle” analysis step. The transition from global to local buckling characterized by a decrease in buckling load and change in the buckled shape of the column is determined for each cross-sectional shape. The point of transition marks the maximum load that can be sustained for that cross-sectional shape. The maximum load for all the cross-sections is determined and compared. The tubular circular cross-section composite column is found to provide the highest buckling load followed by the star with bead cross-section, star shaped cross-section and tubular equilateral triangular cross-section composite column in the respective order. Thus of the shapes considered, the tubular circular cross-section is the optimum shape for the cross-section of the arrow shaft.

Table of Contents

Acknowledgements	iii
Abstract	iv
Table of Contents	v
List of Symbols	vii
List of Figures	viii
List of Tables	xi
Chapter 1 Introduction	01
1.1 Background	01
1.2 Motivation for Research	01
1.3 Objectives and Scope	02
1.4 Outline of Thesis	02
Chapter 2 Literature Survey	04
Chapter 3 Analytical Modeling	07
Chapter 4 Finite Element Analysis	11
4.1 Tubular Circular Cross-Section Composite Column	11
4.2 Tubular Equilateral Triangular Cross-Section Composite Column	21
4.3 Star Shaped Cross-Section Composite Column	26
4.4 Star with Beads Cross-Section Composite Column	30
Chapter 5 Results and Discussion	37
5.1 Tubular Circular Cross-Section Composite Column	40
5.2 Tubular Equilateral Triangular Cross-Section Composite Column	43
5.3 Comparison of Maximum Critical Load for Tubular Circular and Tubular Equilateral Triangular Cross-Sections	45
5.4 Star Shaped Cross-Section Composite Column	47
5.5 Comparison of Maximum Critical Load for the Star Shaped Cross-Section with Tubular Circular and Tubular Equilateral Triangular Cross-Sections	49
5.6 Star with Beads Cross-Section Composite Column	50
5.7 Comparison of Maximum Critical Load for all Cross-Sections	55

Chapter 6 Conclusions and Recommendations	56
References	57
Biographical Information	58

List of Symbols

Roman Symbols:

b column cross section width
 h column cross-section depth
 r radius of circular cross-section

A area of the cross section
 E Young's modulus
 I least area moment of inertia for the column cross-section
 L length of the column
 P load

Subscripts:

cr critical value

List of Figures

Figure 2.1	Arrow with longitudinally extended flutes	05
Figure 2.2	Fluted arrow comprising of 3 lobes	05
Figure 2.3	Tubular elongate shaft with interior walls	06
Figure 4.1	Ply stack plot for the tubular circular cross-section composite column	14
Figure 4.2	Mesh of S8R type tubular circular cross-section composite column	15
Figure 4.3	Mesh of C3D20R type tubular circular cross-section composite column	15
Figure 4.4	Coupling constraints for S8R type tubular circular cross-section composite column	16
Figure 4.5	Constraints to simulate pinned- pinned boundary condition for S8R type tubular circular cross-section composite column	17
Figure 4.6	Constraint to prevent the lateral displacement of S8R type tubular circular cross-section composite column	17
Figure 4.7	Uniform, general shell edge load for predicting buckling load of S8R type tubular circular cross-section composite column	18
Figure 4.8	Beam type multi-point constraints for C3D20R type tubular circular cross-section composite column	19
Figure 4.9	Constraint to prevent the lateral displacement of C3D20R type tubular circular cross-section composite column	19
Figure 4.10	Constraint to simulate pinned-pinned boundary conditions for C3D20R type tubular circular cross-section composite column	20
Figure 4.11	Uniform pressure for predicting the buckling load of C3D20R type tubular circular cross-section composite column	20
Figure 4.12	Ply stack plot for the tubular equilateral triangular cross-section composite column	22

Figure 4.13 Mesh of C3D20R type tubular equilateral triangular cross-section composite column	22
Figure 4.14 Beam type multi-point constraints for C3D20R type tubular equilateral triangular cross-section composite column	23
Figure 4.15 Constrain to prevent the lateral displacement of C3D20R type tubular equilateral triangular cross-section composite column	24
Figure 4.16 Constrains to simulate pinned-pinned boundary conditions for C3D20R type tubular equilateral triangular cross-section composite column	24
Figure 4.17 Uniform pressure for predicting the buckling load of C3D20R type tubular equilateral triangular cross-section composite column	25
Figure 4.18 Ply stack plot for the star shaped cross-section composite column	27
Figure 4.19 Mesh of C3D20R type star shaped cross-section composite column	27
Figure 4.20 Constrain to prevent the lateral displacement of C3D20R type star shaped cross-section composite column	28
Figure 4.21 Constrains to simulate pinned-pinned boundary conditions for C3D20R type star shaped cross-section composite column	28
Figure 4.22 Uniform pressure for predicting the buckling load of C3D20R type star shaped cross-section composite column	29
Figure 4.23 Ply stack plot for the rectangular lobes of star with beads cross-section composite column	33
Figure 4.24 Ply stack plot for the beads of star with beads cross-section composite column	33
Figure 4.25 Mesh of C3D20R type star with beads cross-section composite column	34
Figure 4.26 Constrain to prevent the lateral displacement of C3D20R type star with beads cross-section composite column	35

Figure 4.27 Constrains to simulate pinned-pinned boundary conditions for C3D20R type star with beads cross-section composite column	35
Figure 4.28 Uniform pressure for predicting the buckling load of C3D20R type star with beads cross-section composite column	36
Figure 5.1 Relative area moment of inertia for regular polygonal cross-sections	38
Figure 5.2 Deformed shape for global buckling of composite column	39
Figure 5.3 Plot of critical load vs. thickness for the tubular circular cross-section composite column	42
Figure 5.4 Plot of critical load vs. thickness for the tubular equilateral triangular cross-section composite columns	44
Figure 5.5 Plot of critical load vs. thickness for tubular circular and equilateral triangular cross section composite columns	44
Figure 5.6 Comparison of the critical load vs. thickness for solid and tubular, circular and equilateral triangular cross-section composite columns	46
Figure 5.7 Plot of critical load vs. thickness for star shaped cross-section composite column	48
Figure 5.8 Plot of critical load vs. thickness for tubular equilateral triangular, tubular circular and star shaped cross-section composite columns	49
Figure 5.9 Variation of critical load with radius of beads for star with beads cross-section composite column	53
Figure 5.10 Plot of maximum critical load vs. thickness for star with beads cross section composite column	54
Figure 5.11 Plot of the critical load vs. thickness for all cross-sectional shapes	55

List of Tables

Table 4.1 Variation of thickness and the corresponding shell radius for the S8R type tubular circular cross-section composite column	12
Table 4.2 Variation of thickness and corresponding inner and outer radii for C3D20R type tubular circular cross-section composite column	13
Table 4.3 Variation of thickness and corresponding inner and outer sides for the tubular equilateral triangular cross-section composite column	21
Table 4.4 Variation of thickness and corresponding height of lobes for the star shaped cross section composite column	26
Table 4.5 Variation of radius of beads and the corresponding height of the lobes for thickness = 0.015 inches	30
Table 4.6 Variation of radius of beads and the corresponding height of the lobes for thickness = 0.011 inches	30
Table 4.7 Variation of radius of beads and the corresponding height of the lobes for thickness = 0.010 inches	31
Table 4.8 Variation of radius of beads and the corresponding height of the lobes for thickness = 0.009 inches	31
Table 4.9 Variation of radius of beads and the corresponding height of the lobes for thickness = 0.008 inches	31
Table 4.10 Variation of radius of beads and the corresponding height of the lobes for thickness = 0.007 inches	32
Table 4.11 Variation of radius of beads and the corresponding height of the lobes for thickness = 0.005 inches	32
Table 5.1 Relative area moment of inertia for regular polygonal cross-sections	37
Table 5.2 Critical load for S8R type tubular circular cross-section composite column	40

Table 5.3 Critical load for C3D20R type tubular circular cross-section composite columns	41
Table 5.4 Critical load for C3D20R type tubular equilateral triangular cross-section composite column C3D20R	43
Table 5.5 Critical load for star shaped cross-section composite column	47
Table 5.6 Variation of the critical load with the radius of the bead for thickness = 0.015 in	50
Table 5.7 Variation of the critical load with the radius of the bead for thickness = 0.011 in	51
Table 5.8 Variation of the critical load with the radius of the bead for thickness = 0.010 in	51
Table 5.9 Variation of the critical load with the radius of the bead for thickness = 0.009 in	51
Table 5.10 Variation of the critical load with the radius of the bead for thickness = 0.008 in	52
Table 5.11 Variation of the critical load with the radius of the bead for thickness = 0.007 in	52
Table 5.12 Variation of the critical load with the radius of the bead for thickness = 0.005 in	52
Table 5.13 Maximum critical load for different thicknesses of star with bead cross-section composite column	54

CHAPTER 1

Introduction

1.1 Background

Archery has been in the history of mankind from times immemorial. In ancient times archery was used in warfare and hunting. Currently the dominant use of archery is in hunting, competition sports, including the Olympic Games, and as a recreational sport. Modern archery is a technological sport that combines technology with the art of shooting arrows.

Arrows are shafted projectiles that are shot with a bow. An arrow usually consists of a shaft with an arrowhead attached to the front end, with fletchings and a nock at the other end.

There has been significant advancement in the construction of bows with the use of composites. Historically arrow shafts were made of wood with solid circular cross-sections. Tubular, circular cross-section aluminum shafts replaced the solid wooden shafts with the advent of affordable, aircraft grade aluminum alloys. Arrows commercially available today are made up of composites or a combination of both aluminum and composite materials, and have tubular circular cross-sections. There is scope for the improvement in the cross-sectional design of arrow shafts to increase performance.

1.2 Motivation for Research

Arrows have a high commercial value and the use of composite materials in the field of archery has brought in significant technological advancement. This study aims at improving the target accuracy of a composite arrow while keeping the overall weight of the arrow constant.

One of the factors that negatively affect the target accuracy of the arrows in flight is the phenomenon of dynamic buckling. Due to dynamic buckling, the target accuracy of the arrow may be greatly compromised. For both dynamic and quasi-static buckling, the buckling load depends on the area moment of inertia of the column cross section which should be increased without increasing the weight of the column, by re-distributing the material as far from the principal axis of the cross section as possible, while keeping the material thick enough to prevent local buckling. Hence a quasi-static buckling analysis is carried out in this study and attempts are made to optimize the shape of the composite column cross-section.

1.3 Objectives and Scope

The objective of this study is to optimize using the finite element method the cross sectional shape of a constant cross-sectional area, pinned-pinned composite column subjected to a quasi- static axial compressive load.

A composite column made up of the composite material IM7-8852, having a length of 26 inches and cross sectional area of 0.0212058 in² is analyzed in this study. The length and cross-sectional area of the composite column were taken from a sample composite arrow manufactured by “Victory Archery” having an inner and outer diameter of 0.245 inches and 0.295 inches respectively. Four cross-sectional shapes: tubular circular, tubular equilateral triangular, star shaped and star with beads are analyzed in this study.

1.4 Outline of Thesis

A literature survey is conducted on the relevant technologies related to arrow shafts and summarized in Chapter 2, followed by the analytical modeling in Chapter 3 wherein an analytical expression for the prediction of global buckling load for three of the four cross-sections is introduced. Chapter 4 details the steps involved in the finite element modeling of the composite column using ABAQUS . The results are

presented and discussed in Chapter 5. The conclusions followed by the recommendations for future work are covered in Chapter 6.

CHAPTER 2

Literature Survey

There has been significant technological improvement in the field of archery with the use of composite materials. Composite materials have a high specific strength and specific stiffness, which is desirable in the construction of bows and arrows. This has led to the development of modern compound bows and composite arrows. In this chapter, prior research conducted on the buckling of arrow shafts is summarized. Some of the patents, related to the change in cross-sectional shape of the arrow shaft are also discussed to emphasize the commercial importance of this study.

References 1-4 represent the relevant technical publications addressing mechanics of the bow and arrow system.

In these references, the vibration response of a tubular circular arrow shaft during and after being fired from the bow is analysed. However little effort has been made to fully prevent the vibrations of the arrow shaft by eliminating dynamic buckling. This study discusses the possible cross-sectional shapes that can prevent the buckling of arrow shafts thereby avoiding the excitation of lateral vibrations in arrows. This work is relevant to arrows shot from a compound and centershot bow for which the phenomenon of dynamic buckling is undesirable.

References 5-7 represent US Patents that are related to variation in cross-sectional shape of the arrow shaft.

In Ref. 5 (US Patent 5,273,293) an arrow with longitudinally extended flutes as shown in Fig. 2.1 is disclosed.

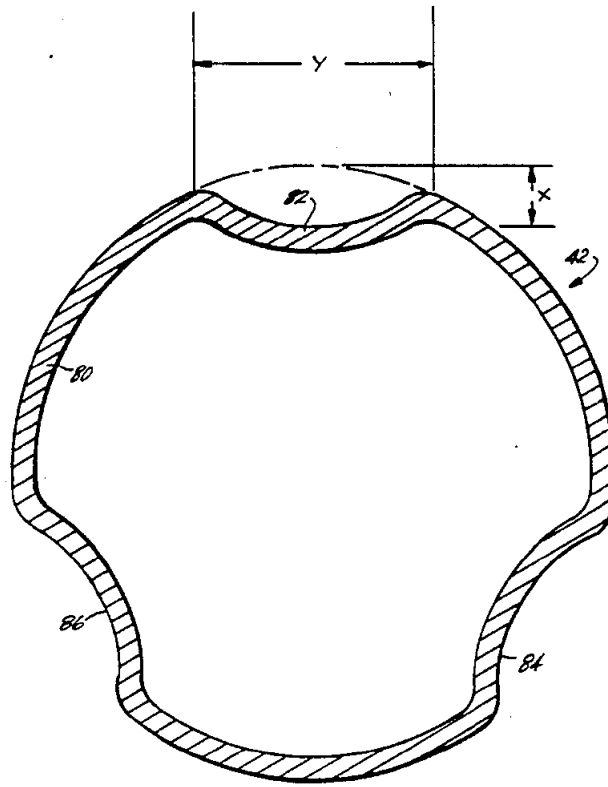


Figure 2.1 Arrow with longitudinally extended flutes (Ref. 5)

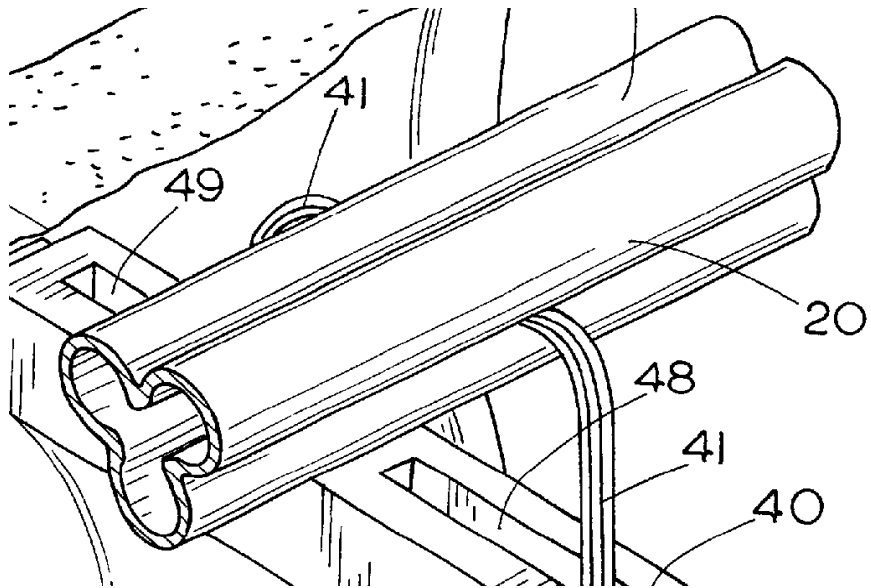


Figure 2.2 Fluted arrow comprising of 3 lobes (Ref. 6)

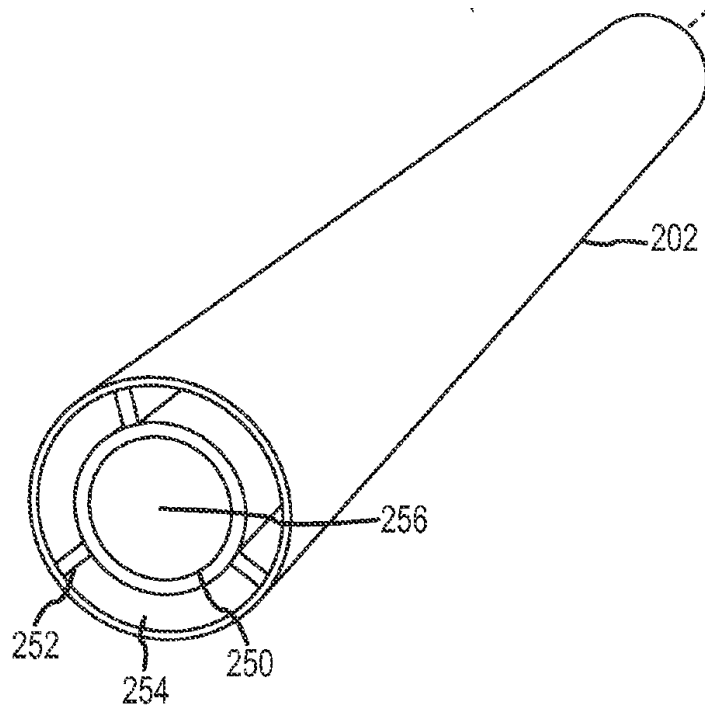


Figure 2.3 Tubular elongate shaft with interior walls (Ref. 7)

In Ref. 6 (US Patent 6,595,880) a fluted arrow as shown in Fig. 2.2, comprising of three lobes on its cross-section is disclosed.

In Ref. 7 (US Patent 8,915,806) an arrow comprising of a tubular elongate shaft that has interior walls which intersect the shaft at rounded edge as shown in Fig. 2.3 is disclosed.

In all the above mentioned patents, the cross sectional shape of the arrow shaft is modified and it is claimed that a higher target accuracy and reduction in weight can be achieved. However, these claims are not supported by any technical proof.

CHAPTER 3

Analytical Modeling

The purpose of this chapter is to introduce an analytical model that is used for accurately predicting the global buckling load of a constant area, pinned-pinned composite column with fibers oriented along the length of the column.

Buckling can be defined as the phenomenon of structural instability, characterized by the occurrence of adjacent equilibrium positions. Euler derived the formula that gives the maximum axial load at which a pinned-pinned, slender, ideal column buckles. It is given by

$$P_{cr} = \frac{\pi^2 EI}{L^2} \quad (3.1)$$

where,

P_{cr} : critical load

E : Young's modulus

I : least area moment of inertia for the cross section

L : length of the column

An ideal column is one that is perfectly straight, homogeneous and free from initial stress. The formula to predict the buckling load for a pinned-pinned composite column with fibers oriented along its length is given by:

$$P_{cr} = \frac{\pi^2 E_1 I}{L^2} \quad (3.2)$$

Where,

P_{cr} : critical load

E_1 : modulus of elasticity along the longitudinal direction

I: least area moment of inertia for the cross section

L: length of the composite column

When subjected to an axial compressive load, the column buckles about the principal axis having the least area moment of inertia. Hence cross sectional shapes having centroids as principal points are considered in this study.

All regular polygons have centroids as principal points. Hence solid regular polygonal cross-sections with varying number of sides are analyzed. The circle is considered as the limiting case of a regular polygon with an infinite number of sides.

The area moment of inertia for a solid regular polygonal cross-section about the principal centroidal axis as given in Ref. 8:

$$I_{regular_polygon} = \frac{nb^4}{192} \cot\left(\frac{180}{n}\right) \left(3 \cot^2\left(\frac{180}{n}\right) + 1\right) \quad (3.3)$$

where

b: base length of the regular polygon

n: number of sides of the regular polygon ($n \geq 3$)

The relation between the side length (b) and the area (A) for an n sided regular polygon is given by the expression:

$$b = \left(\frac{4A}{n} \tan\left(\frac{180}{n}\right)\right)^{\frac{1}{2}} \quad (3.4)$$

Substituting (3.4) in (3.3), the area moment of inertia for an n sided solid regular polygonal cross-section about the principal centroidal axis can be expressed as:

$$I_{regular_polygon} = \frac{A^2}{12n} \left(\cot\left(\frac{180}{n}\right) \right) \left(\tan^2\left(\frac{180}{n}\right) + 3 \right) \quad (3.5)$$

The area moment of inertia for a solid circular cross-section in terms of area (A) is:

$$I_{circle} = \frac{A^2}{4\pi} \quad (3.6)$$

Normalizing the area moment of inertia for the circle and maintaining the area constant, the relative area moment of inertia for an n sided regular polygon about the principal centroidal axis is expressed as follows:

$$I_{relative_regular_polygon} = \frac{\pi}{3n} \left(\cot\left(\frac{180}{n}\right) \right) \left(\tan^2\left(\frac{180}{n}\right) + 3 \right) \quad (3.7)$$

Using the above expression, the area moment of inertia for the solid circular cross-section is compared with that for solid regular polygonal cross-sections having sides 3, 4, 5 and 6. It is shown that for a given cross-sectional area, a solid equilateral triangular cross-section has a higher area moment of inertia than a solid circular cross-section.

Based on this result, the tubular circular cross-section arrow shaft is compared with a tubular equilateral triangular cross-section shaft with the expectation that the tubular equilateral triangular cross-section shaft will exhibit a higher buckling load and hence will be a better shape for the arrow cross-section. Further, a star shaped cross-section will be analyzed followed by a star with bead cross-section and the optimum shape will be determined.

For the tubular circular, tubular equilateral triangular and star shaped cross-section composite columns, the thickness of the column cross section is varied and the corresponding critical load is determined. For the star with beads cross-section composite column, the thickness and radius of the beads are varied.

For the analytical prediction of buckling load, the area moment of inertia for a tubular circular cross section about the principal centroidal axis is given by:

$$I = \frac{\pi(r_1^4 - r_2^4)}{4} \quad (3.8)$$

The area moment of inertia for a tubular equilateral triangular cross-section about the principal centroidal axis is given by:

$$I = \frac{\sqrt{3}(b_1^4 - b_2^4)}{96} \quad (3.9)$$

The expression for the area moment of inertia for the star shaped cross-section is derived to be:

$$I = \frac{bh^3}{8} + \frac{hb^3}{12} + bh\left(\frac{h}{2} + \frac{b}{2\sqrt{3}}\right)^2 + \frac{\sqrt{3}b^4}{96} \quad (3.10)$$

where,

b: side length of the equilateral triangle at the center,

h: height of the three rectangular lobes measured from the base of the triangle.

For the star with beads cross-section composite column, only the finite element method is used in the prediction of buckling load.

CHAPTER 4

Finite Element Analysis

Finite element method solutions predicting the buckling load of composite column were obtained for four different cross-sectional shapes in ABAQUS. The length and area of the cross-section are taken to be 26 inches and 0.0212058 in² respectively. The material of the column is assumed to be IM7-8552. The area of the cross-section is assumed to be uniform along the length of the column. The material properties used in this analysis are: $E_1 = 22.99$ Msi, $E_2 = 1.3$ Msi, $E_3 = 1.3$ Msi, $\nu_{12} = 0.316$, $\nu_{13} = 0.316$, $\nu_{23} = 0.316$, $G_{12} = 0.69$ Msi, $G_{13} = 0.69$ Msi, $G_{23} = 0.43$ Msi. A “Linear Perturbation, Buckle” analysis was used in ABAQUS to predict the buckling load of the composite arrow shaft.

4.1 Tubular Circular Cross- Section Composite Column

The thickness of the tubular circular cross-section composite column was varied, keeping the length and area of the cross-section constant.

The tubular circular cross-section composite column was modeled in ABAQUS using the S8R (8 noded doubly curved thick shell, reduced integration) and C3D20R (20 noded quadratic brick element, reduced integration) element types.

The variation of the thickness and the corresponding shell radius used to model the tubular circular cross-section composite column using S8R element type is shown in Table 4.1.

The variation of the thickness and the corresponding inner and outer radii used to model the tubular circular cross-section composite column using C3D20R element type is shown in Table 4.2

Table 4.1: Variation of the thickness and the corresponding shell radius for S8R type tubular circular cross-section composite column

Thickness (in)	Shell Radius (in)
0.0250	0.135000
0.0200	0.168750
0.0150	0.225000
0.0100	0.337500
0.0093	0.362904
0.0087	0.387932
0.0084	0.401787
0.0081	0.416668
0.0078	0.432693
0.0077	0.438313
0.0076	0.44408
0.0075	0.450000
0.0050	0.675000

Table 4.2: Variation of the thickness and the corresponding inner and outer radii for C3D20R type tubular circular cross-section composite column

Thickness (in)	Inner Radius (in)	Outer Radius (in)
0.0820	0.000159	0.082159
0.0810	0.001167	0.082167
0.0800	0.002188	0.082188
0.0750	0.007500	0.082500
0.0700	0.013214	0.083214
0.0650	0.019423	0.084423
0.0600	0.026250	0.086250
0.0550	0.033864	0.088864
0.0500	0.042500	0.092500
0.0450	0.052500	0.097500
0.0400	0.064375	0.104375
0.0350	0.078929	0.113929
0.0300	0.097500	0.127500
0.0250	0.122500	0.147500
0.0200	0.158750	0.178750
0.0150	0.217501	0.232501
0.0100	0.332501	0.342501
0.0093	0.358254	0.367554
0.0087	0.383582	0.392282
0.0084	0.397587	0.405987
0.0081	0.412618	0.420718
0.0078	0.428793	0.436593
0.0077	0.434463	0.442163
0.0076	0.440280	0.447880
0.0075	0.446251	0.453751
0.0050	0.672502	0.677502

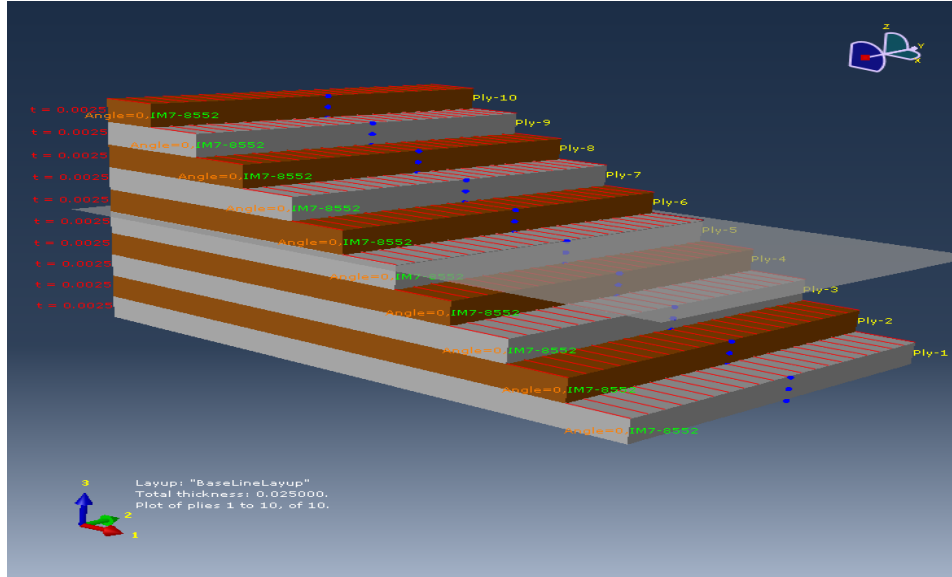


Figure 4.1 Ply stack plot for the tubular circular cross-section composite column

Ten equal plies each having a thickness of one-tenth the wall thickness and 0^0 fiber orientation were used to model the composite column as shown in Fig. 4.1. In this study, thickness is considered to be a continuous variable, although from a practical standpoint thickness can only be an integer multiple of individual ply thickness.

4.1.1 Meshing

The mesh of the tubular circular cross-section composite column modeled using S8R element type is shown in Fig. 4.2. The number of elements used to mesh the composite column using S8R element type to obtain a converged solution is 6360. The maximum aspect ratio in the modeling of the composite column is less than 10.

The mesh of the tubular circular cross-section composite column modeled using C3D20R element type is shown in Fig. 4.3. The number of elements used to mesh the composite column using C3D20R element type to obtain a converged solution is 8840. The maximum aspect ratio in the meshing of the composite column is 10.

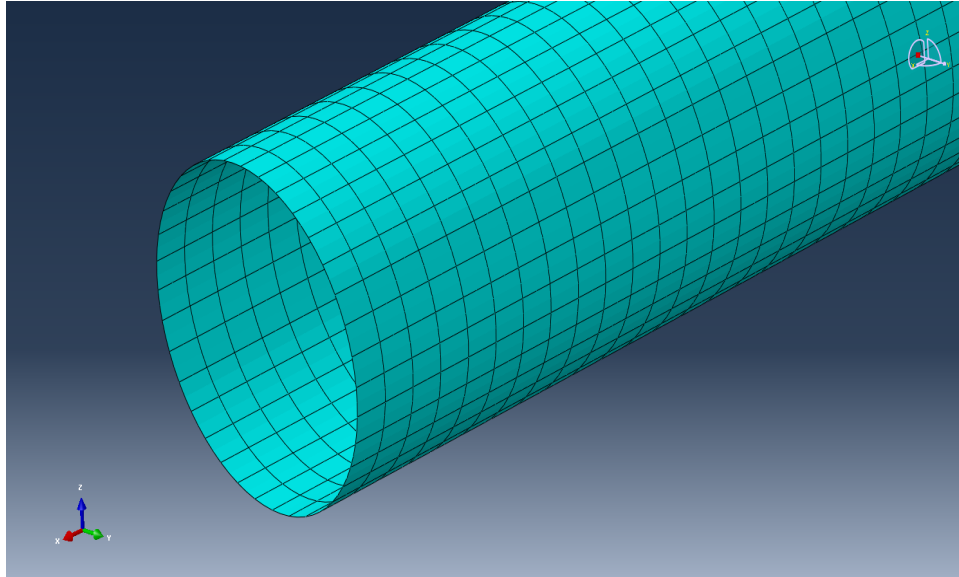


Figure 4.2 Mesh of S8R type tubular circular cross-section composite column

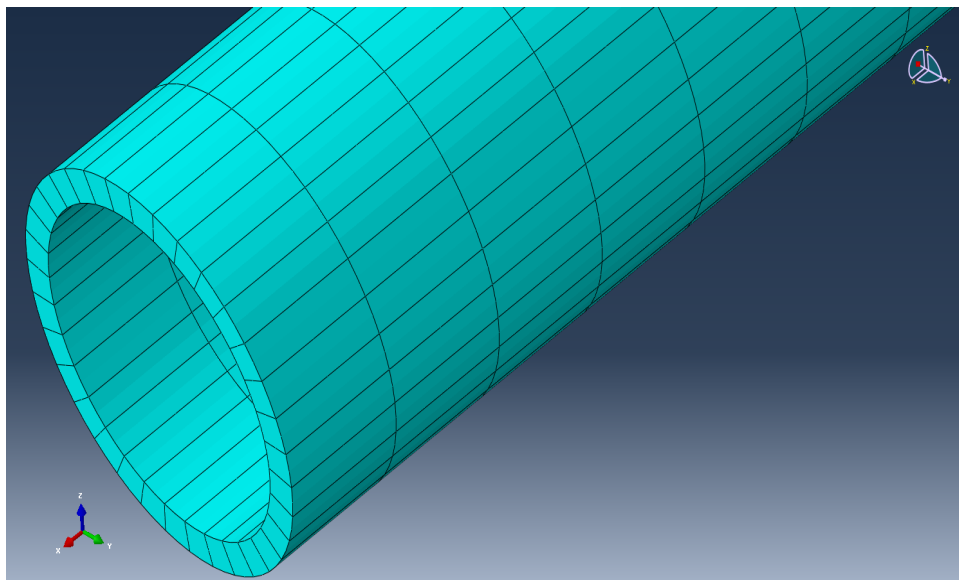


Figure 4.3 Mesh of C3D20R type tubular circular cross-section composite column

4.1.2 Applied Load and Boundary Conditions

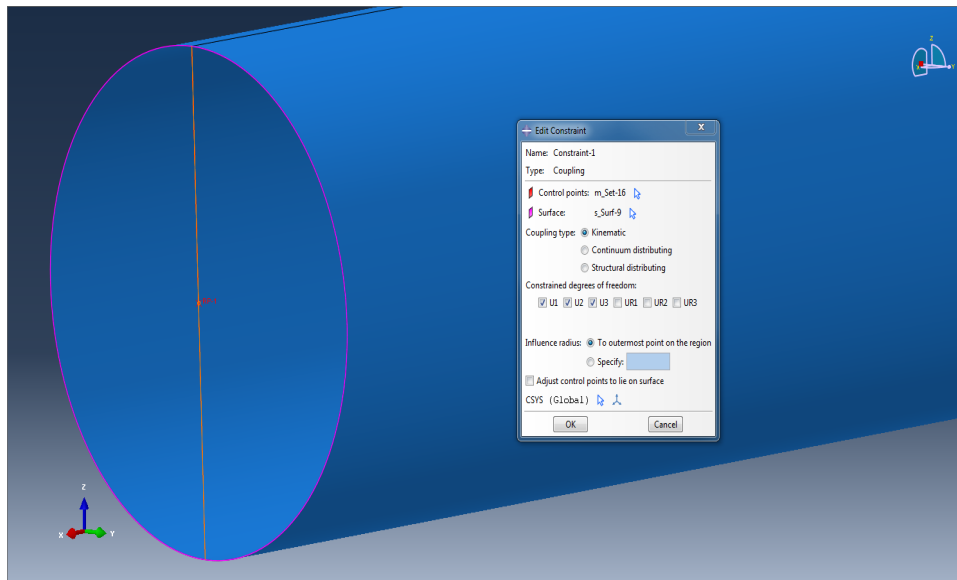


Figure 4.4 Coupling constraints for S8R type tubular circular cross-section composite column

Pinned-pinned boundary conditions are imposed on the tubular circular cross-section composite column. For the modeling of the composite column using shell elements a “coupling” constraint is used in ABAQUS to constrain the edges of one end of the column with respect to the center of the circular cross-section as shown in Fig 4.4.

The displacements along the y and z directions were constrained at both ends of the composite column as shown in Fig. 4.5 to simulate the pinned-pinned boundary condition. At the bottom surface of the column the displacements along the x, y and z directions were constrained about the center as shown in Fig. 4.6, to prevent the lateral displacement of the column.

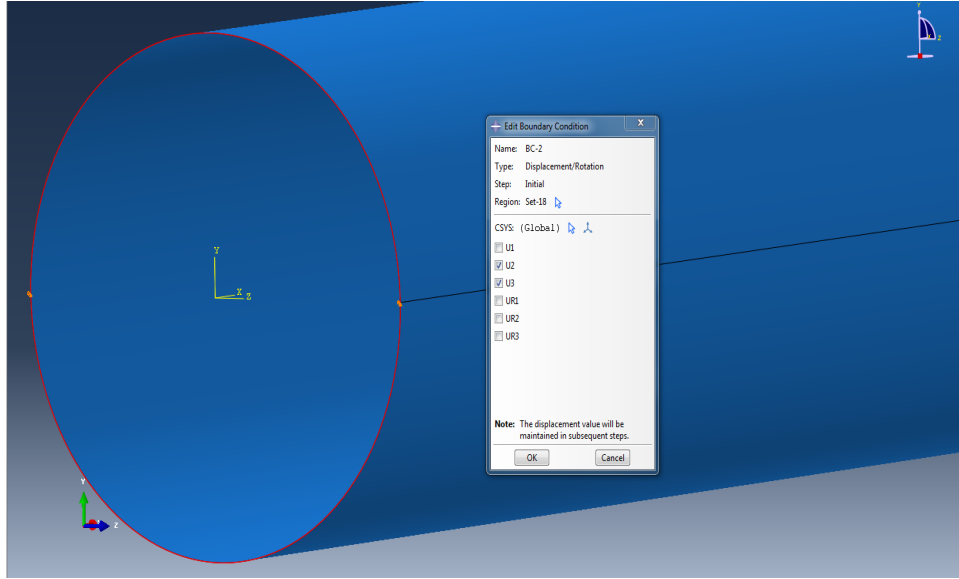


Figure 4.5 Constrains to simulate pinned- pinned boundary conditions for S8R type tubular circular cross-section composite column

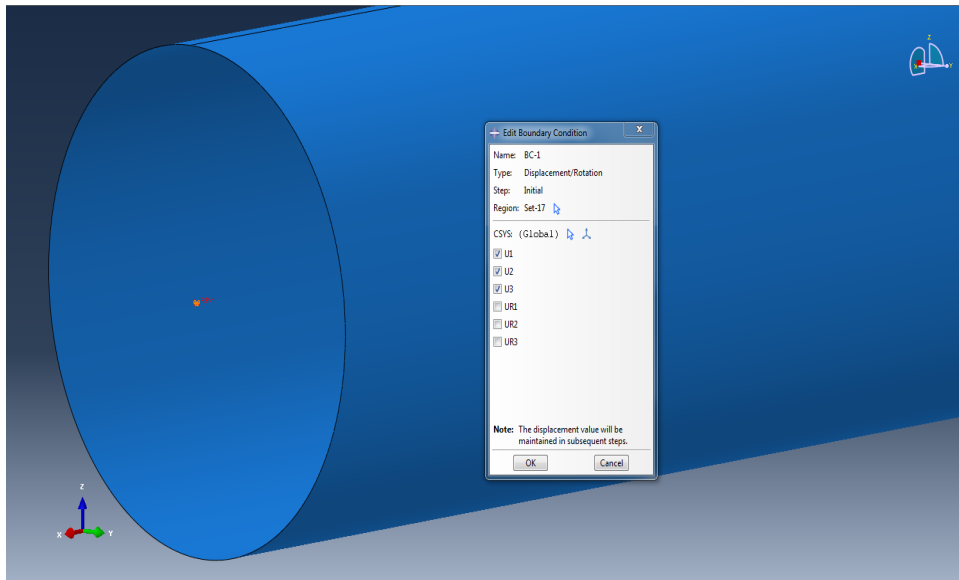


Figure 4.6 Constraint to prevent the lateral displacement of S8R type tubular circular cross-section composite column

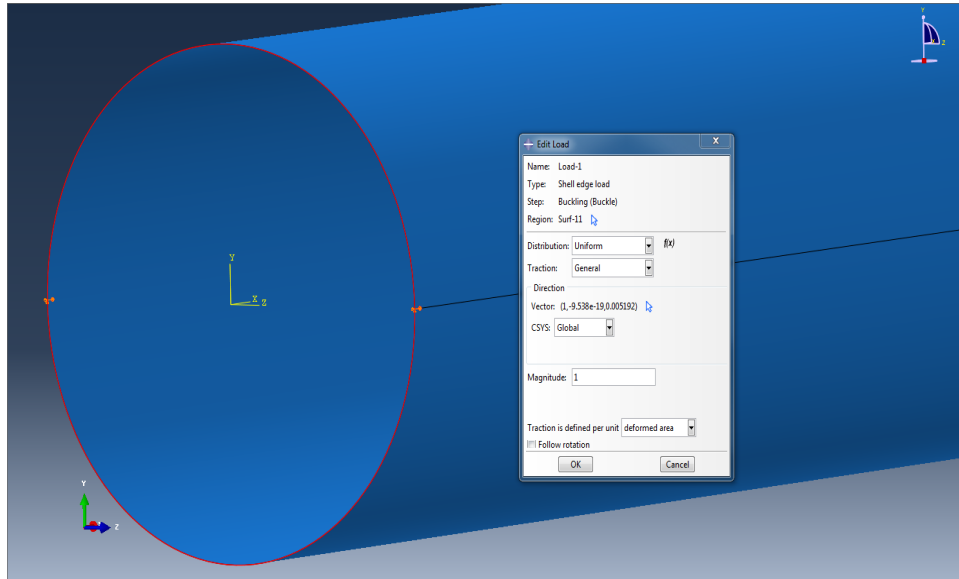


Figure 4.7 Uniform, general shell edge load for predicting buckling load of S8R type tubular circular cross-section composite column

A uniform, general shell edge load of unit magnitude is applied to top edge of the tubular circular cross-section composite column as shown in Fig. 4.7, for the prediction of buckling load.

For the tubular circular cross-section composite column modeled using C3D20R type elements, the surface at one end of the composite column, is constrained about the center of the circle using the “beam” type multi-point constraints as shown in Fig. 4.8 and the x, y and z displacements about that point are constrained as shown in Fig 4.9 to prevent the lateral displacement of the composite column.

The displacements along the y and z directions were constrained at both ends of the composite column as shown in Fig. 4.10 to effectively simulate the pinned-pinned boundary condition.

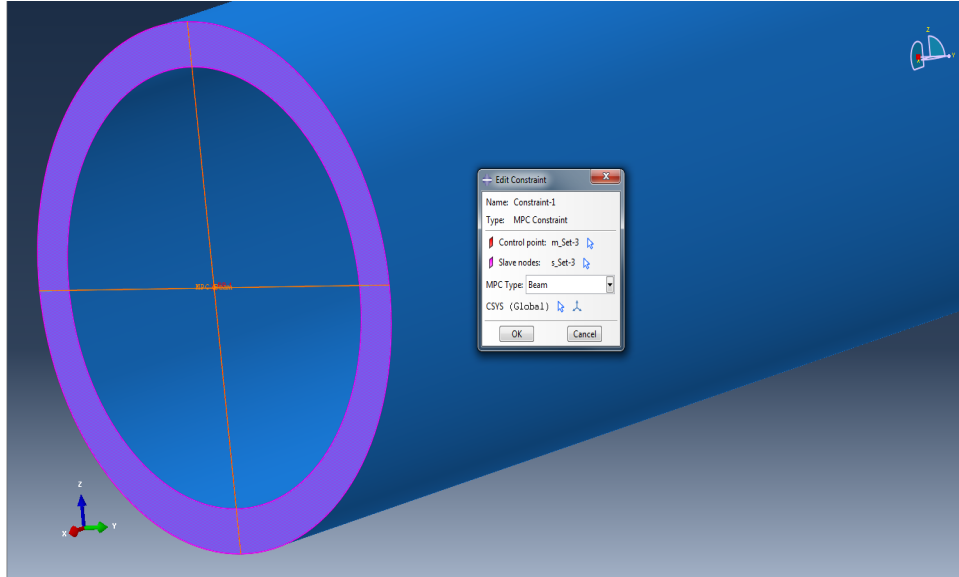


Figure 4.8 Beam type multi-point constraints for C3D20R type tubular circular cross-section composite column

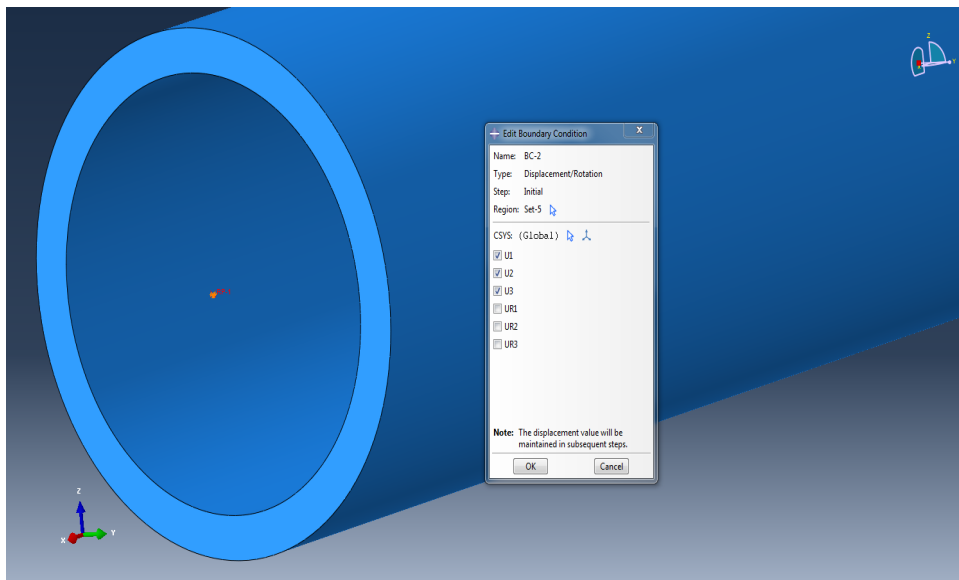


Figure 4.9 Constrain to prevent the lateral displacement of C3D20R type tubular circular cross-section composite column

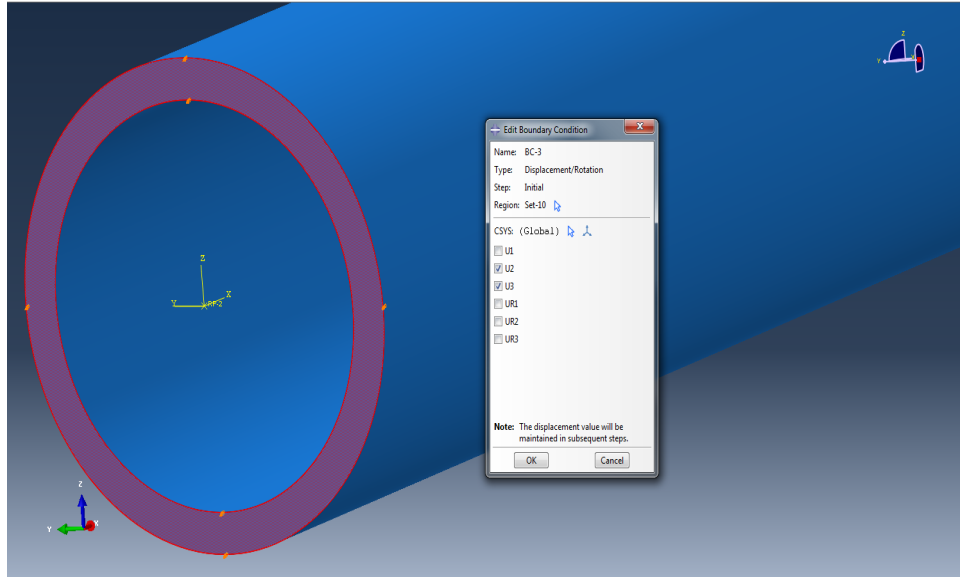


Figure 4.10 Constrains to simulate pinned-pinned boundary conditions for C3D20R type tubular circular cross-section composite column

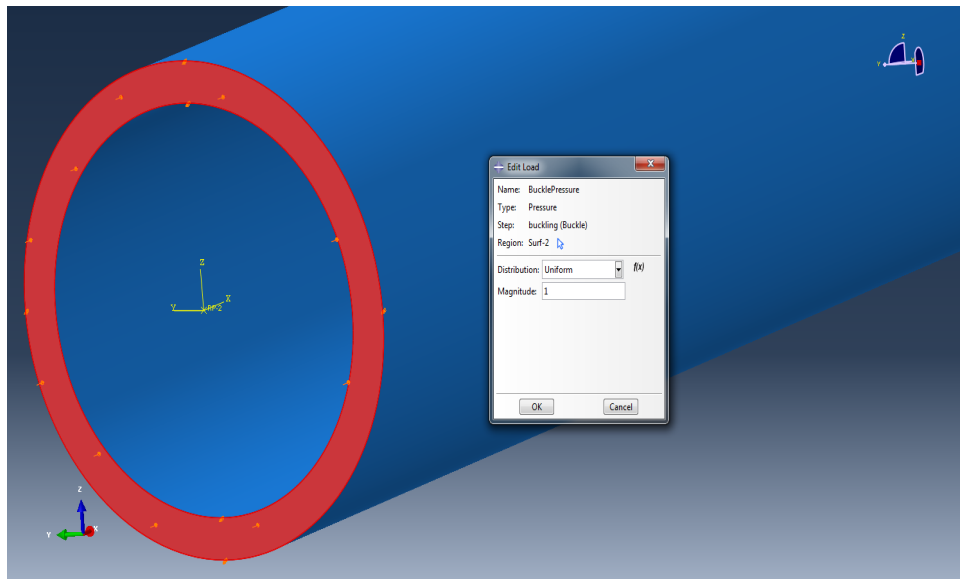


Figure 4.11 Uniform pressure for predicting buckling load of C3D20R type tubular circular cross-section composite column

A uniform pressure of unit magnitude is applied at the top surface of the composite column as shown in Fig. 4.11, to predict the buckling load for the tubular circular cross-section composite column.

4.2 Tubular Equilateral Triangular Cross-Section Composite Column

The tubular equilateral triangular cross-section composite column was modeled in ABAQUS using the C3D20R (20 noded quadratic brick element, reduced integration) element type.

The variation of thickness and the corresponding inner and outer sides used to model the composite column is shown in Table 4.3.

Table 4.3: Variation of thickness and corresponding inner and outer sides for the tubular equilateral triangular cross-section composite column

Thickness (in)	Inner Side (in)	Outer Side (in)
0.0638	0.000288	0.221298
0.063	0.003081	0.221319
0.0620	0.006623	0.221397
0.0610	0.010224	0.221534
0.0600	0.013887	0.221733
0.0550	0.033257	0.223783
0.0500	0.054769	0.227975
0.045	0.079138	0.235022
0.0400	0.107433	0.245997
0.0350	0.141338	0.262582
0.0300	0.183658	0.287582
0.0250	0.239443	0.326045
0.0200	0.318789	0.388071
0.0150	0.445259	0.497221
0.0145	0.462375	0.512604
0.0140	0.480651	0.529149
0.0135	0.500217	0.546983
0.0130	0.521222	0.566255
0.0129	0.525610	0.570297
0.0128	0.530064	0.574405
0.0127	0.534586	0.578580
0.0126	0.539176	0.582824
0.0125	0.543837	0.587139
0.0100	0.689539	0.724181

Ten equal plies each having a thickness of one-tenth the wall thickness and 0° fiber orientation were used to model the composite column as shown in Fig. 4.12.

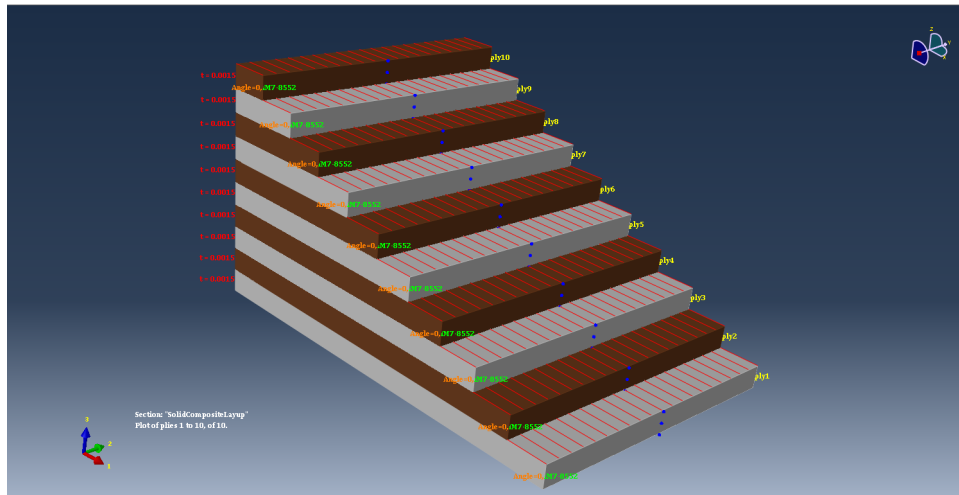


Figure 4.12 Ply stack plot for the tubular equilateral triangular cross-section composite column

4.2.1 Meshing

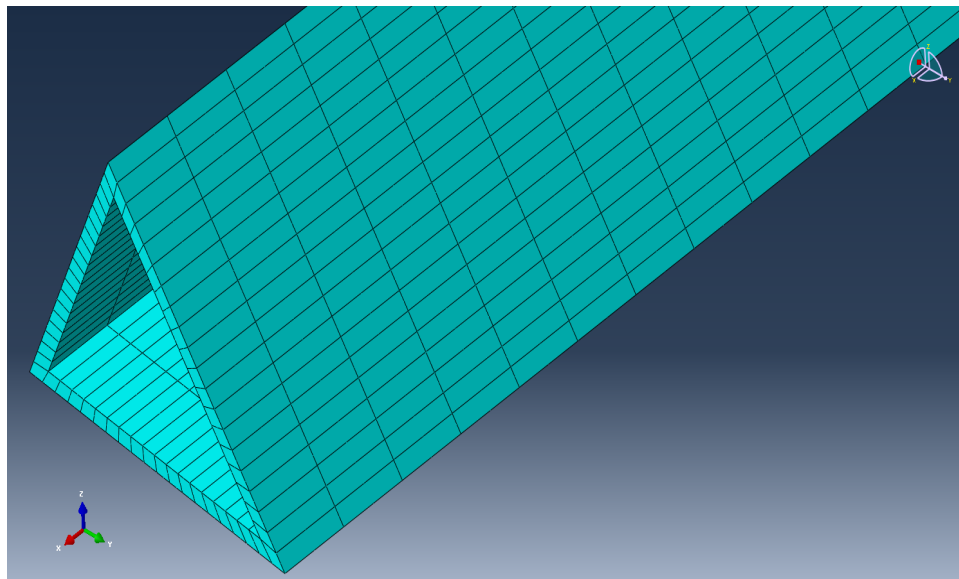


Figure 4.13 Mesh of C3D20R type tubular Equilateral triangular cross-section composite column

The mesh of the tubular equilateral triangular cross-section composite column modeled using C3D20R element type is shown in Fig. 4.13. The number of elements used to mesh the composite column to obtain a converged solution is 19494. The maximum aspect ratio in the modeling of the composite column is 10.

4.1.2 Applied Load and Boundary Conditions

Pinned-pinned boundary conditions are imposed on the tubular equilateral triangular cross-section composite column. The surface at one end of the composite column is constrained about the centroid of the triangle using the “beam” type multi-point constrains as shown in Fig. 4.14. The x, y and z direction displacements are constrained about the centroid as shown in Fig 4.15 to prevent the lateral displacement of the composite column.

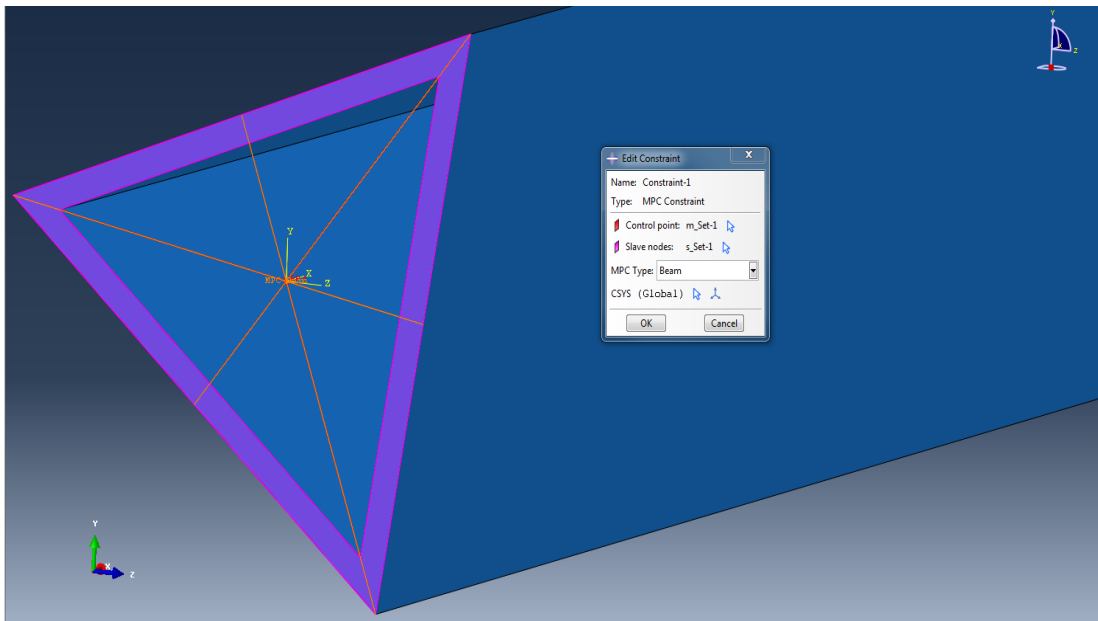


Figure 4.14 Beam type multi-point constraint for C3D20R type tubular equilateral triangular cross-section composite column

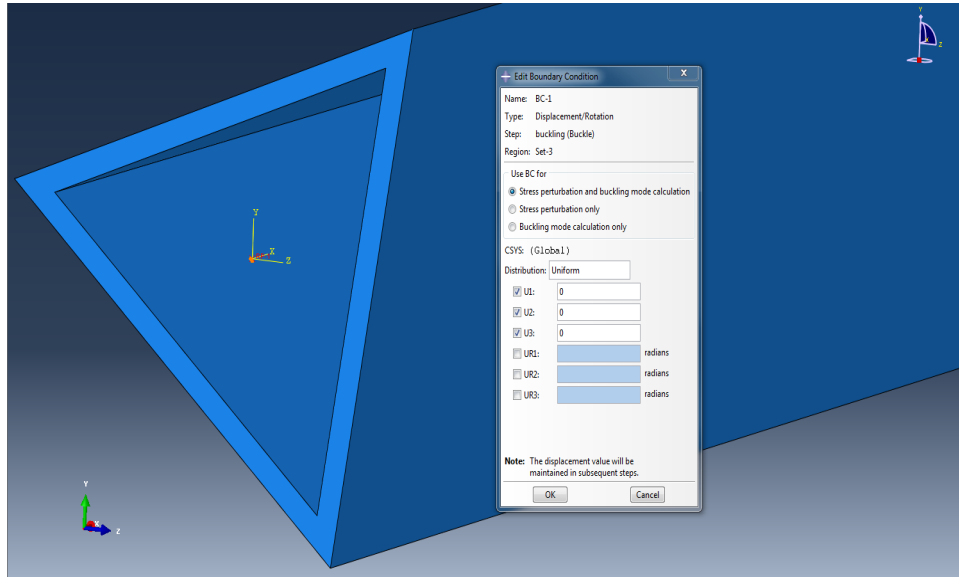


Figure 4.15 Constrain to prevent the lateral displacement of C3D20R type tubular equilateral triangular cross-section composite column

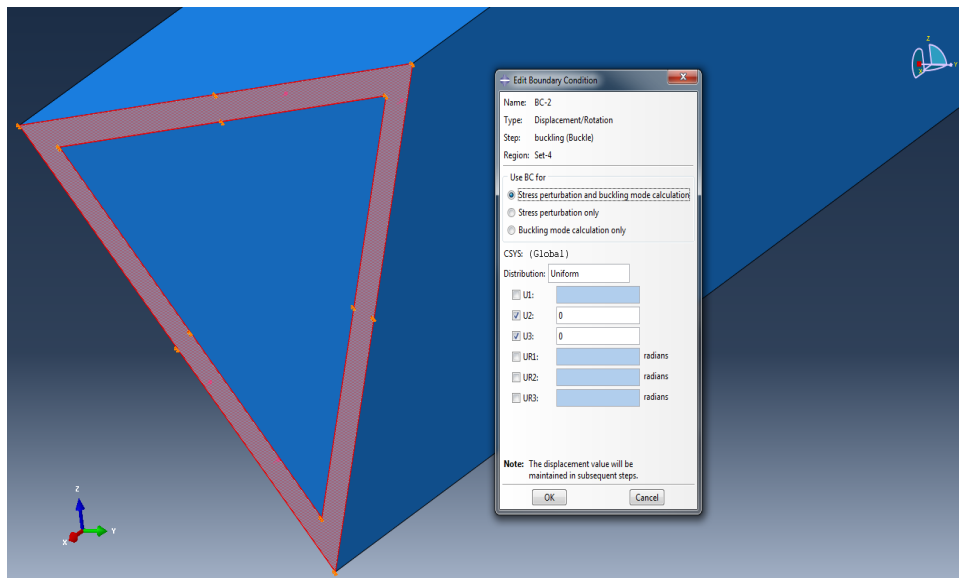


Figure 4.16 Constrains to simulate pinned-pinned boundary conditions for C3D20R type tubular equilateral triangular cross-section composite column

The displacements along the y and z directions were constrained at both ends of the composite column as shown in Fig. 4.16 to effectively simulate the pinned-pinned boundary conditions.

A uniform pressure of unit magnitude is applied at the top surface of the composite column as shown in Fig. 4.17, under the “Linear Perturbation, Buckle” analysis step to predict the buckling pressure and thereby predict the buckling load for the tubular equilateral triangular cross-section composite column.

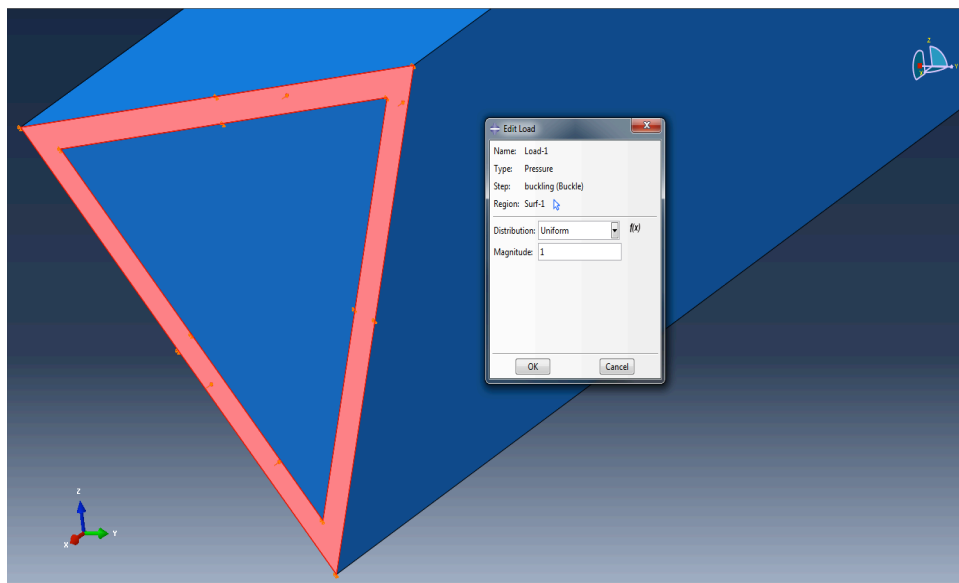


Figure 4.17 Uniform pressure for predicting the buckling load of C3D20R type tubular equilateral triangular cross-section composite column

4.3 Star Shaped Cross-Section Composite Column

The star shaped cross section composite column was modeled in ABAQUS using the C3D20R (20 noded quadratic brick element, reduced integration) element type.

The thickness of the star shaped cross section composite column was varied, keeping the length of the column and area of the cross-section constant. The variation of thickness and the corresponding height of the rectangular lobes used to model the composite columns are shown in Table 4.4.

Table 4.4: Variation of thickness and corresponding height of the lobes for the star shaped cross section composite column

Thickness (in)	Height (in)
0.221298	0.000000
0.220000	0.000376
0.200000	0.006475
0.150000	0.025473
0.100000	0.056252
0.050000	0.134155
0.040000	0.170941
0.030000	0.231290
0.020000	0.350543
0.019000	0.369289
0.018000	0.390102
0.017000	0.413346
0.016000	0.439478
0.015000	0.469075
0.010000	0.705417
0.005000	1.412998

Ten equal plies each having a thickness of one-tenth the wall thickness and 0^0 fiber orientation were used to model the composite column as shown in Fig. 4.18.

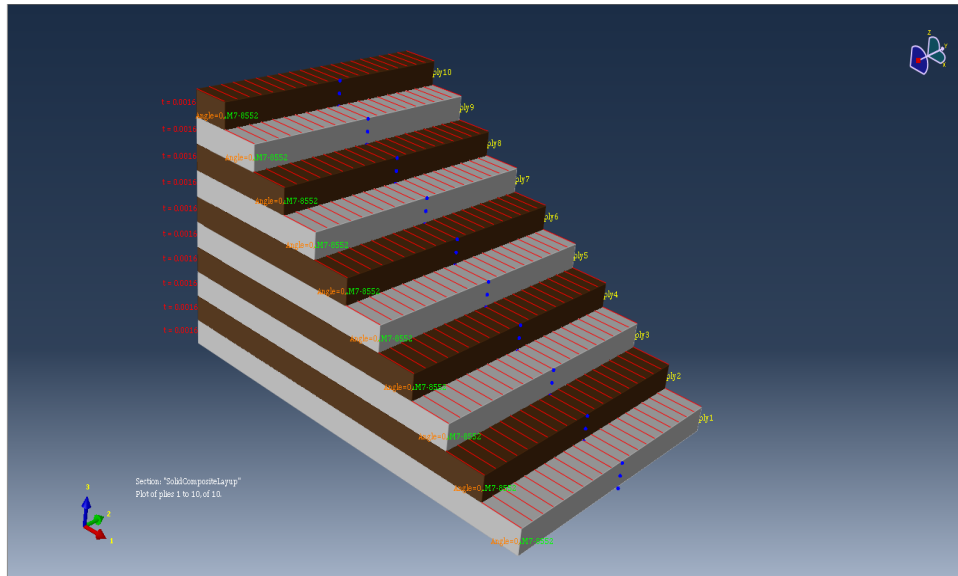


Figure 4.18 Ply stack plot for the star shaped cross-section composite column

4.2.1 Meshing

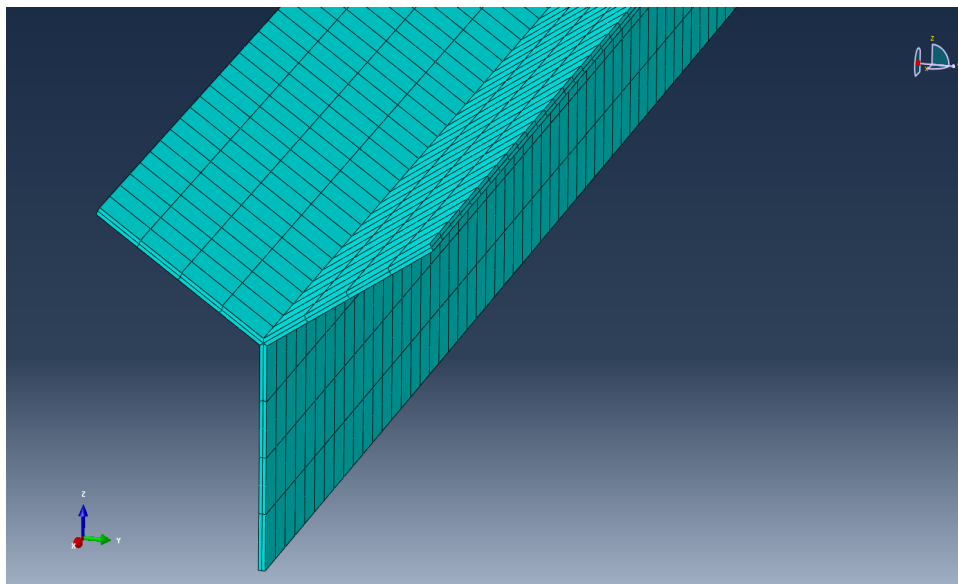


Figure 4.19 Mesh of C3D20R type star shaped cross-section composite column

The mesh for the star shaped cross-section composite column modeled using C3D20R element type is shown in Fig. 4.19. The maximum aspect ratio in the meshing of the star shaped cross-section composite column is 10.

4.1.2 Applied Load and Boundary Conditions

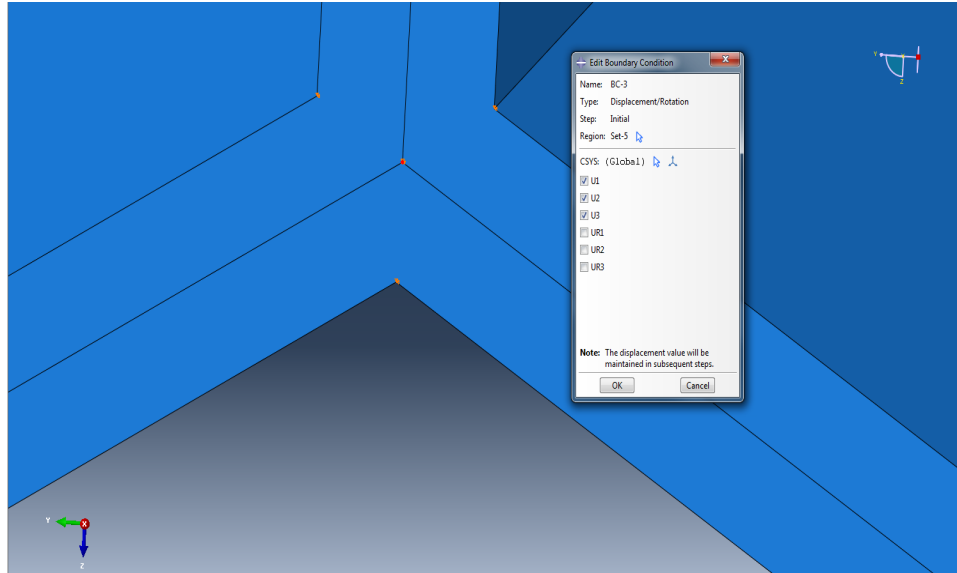


Figure 4.20 Constrain to prevent the lateral displacement of C3D20R type star shaped cross-section composite column

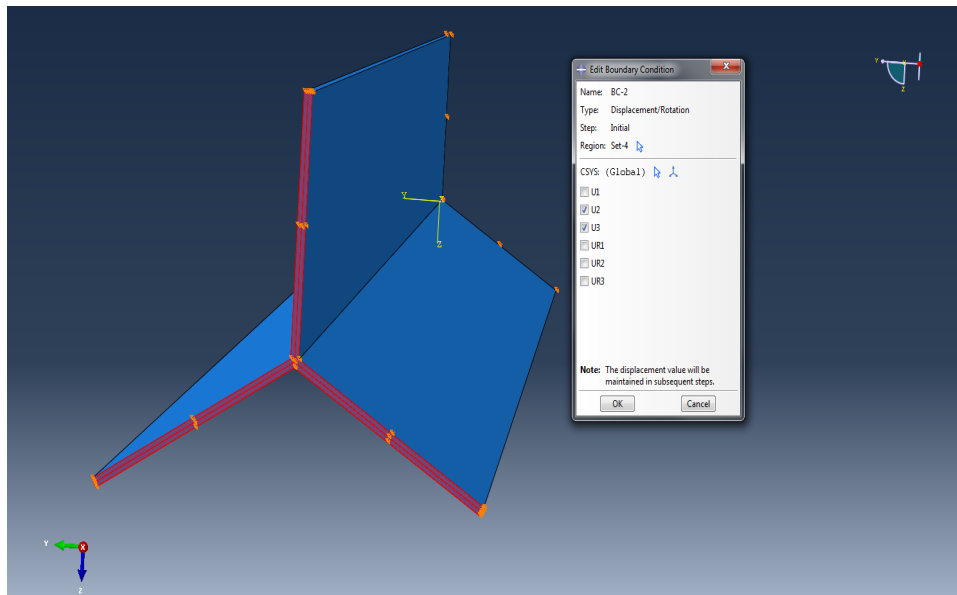


Figure 4.21 Constrains to simulate pinned-pinned boundary conditions for C3D20R type star shaped cross-section composite column

Pinned-pinned boundary conditions are imposed on the star shaped cross-section composite column. The x, y and z displacements about the centroid are constrained as shown in Fig 4.20 to prevent the lateral displacement of the composite column.

The displacements along the y and z directions were constrained at both ends of the composite column as shown in Fig. 4.21 to effectively simulate the pinned-pinned boundary condition.

A uniform pressure of unit magnitude is applied at the top surface of the composite column as shown in Fig. 4.22 under the “Linear Perturbation, Buckle” analysis step to predict the buckling load for the star shaped cross-section composite column

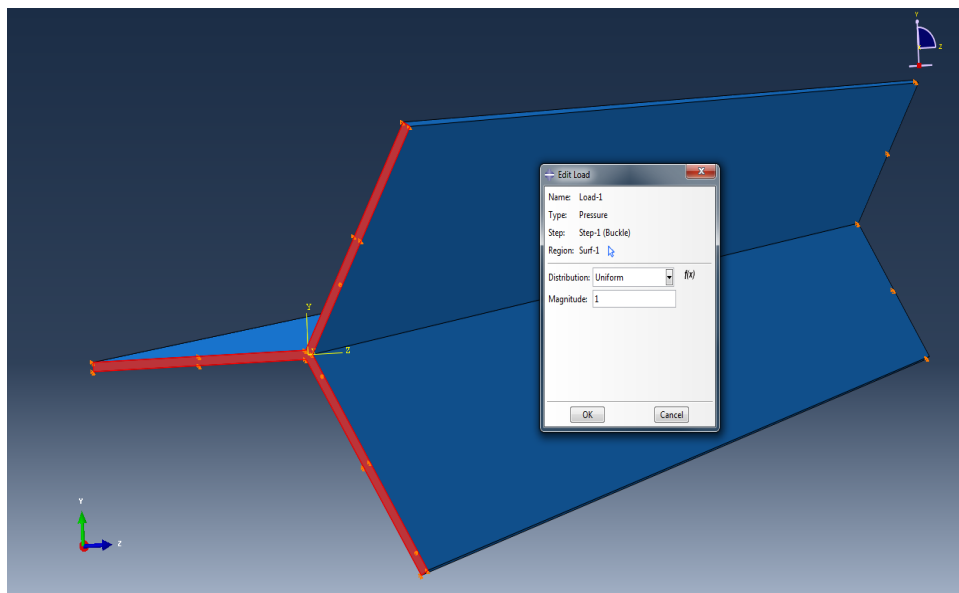


Figure 4.22 Uniform pressure for predicting the buckling load of star shaped cross-section composite column

4.4 Star With Beads Cross-Section Composite Column

The star with beads cross-section composite column was modeled in ABAQUS using the C3D20R (20 noded quadratic brick element, reduced integration) element type.

The radius of the beads was varied for different values of thickness, keeping the length of the column and area of the cross-section constant. The variation of radius of the beads and the corresponding height of the lobes for different values of thicknesses are shown in Tables 4.5 – 4.11.

Table 4.5: Variation of radius of beads and the corresponding height of the lobes for thickness = 0.015 inches

Thickness (in)	Radius of Bead (in)	Height (in)
0.015000	0.015000	0.436300
0.015000	0.018000	0.418681
0.015000	0.019500	0.408444
0.015000	0.022500	0.385122
0.015000	0.030000	0.310264
0.015000	0.045000	0.089751

Table 4.6: Variation of radius of beads and the corresponding height of the lobes for thickness = 0.011 inches

Thickness (in)	Radius of Bead (in)	Height (in)
0.011000	0.029700	0.418617
0.011000	0.030800	0.400717
0.011000	0.031900	0.382125
0.011000	0.033000	0.362841
0.011000	0.034100	0.342866

Table 4.7: Variation of radius of beads and the corresponding height of the lobes for
thickness = 0.010 inches

Thickness (in)	Radius of Bead (in)	Height (in)
0.010000	0.027000	0.503239
0.010000	0.030000	0.452534
0.010000	0.031000	0.434375
0.010000	0.033000	0.396170
0.010000	0.034000	0.376126
0.010000	0.040000	0.242657

Table 4.8: Variation of radius of beads and the corresponding height of the lobes for
thickness = 0.009 inches

Thickness (in)	Radius of Beads(in)	Height (in)
0.009000	0.033300	0.449961
0.009000	0.034200	0.430224
0.009000	0.034200	0.409921
0.009000	0.035100	0.389052
0.009000	0.036000	0.367618
0.009000	0.036900	0.345618
0.009000	0.037800	0.323052

Table 4.9: Variation of radius of beads and the corresponding height of the lobes for
thickness = 0.008 inches

Thickness (in)	Radius of Beads (in)	Height (in)
0.008000	0.035200	0.430975
0.008000	0.036000	0.409408
0.008000	0.036800	0.387339
0.008000	0.037600	0.364767
0.008000	0.038400	0.341692
0.008000	0.039200	0.318115
0.008000	0.040000	0.294035

Table 4.10: Variation of radius of beads and the corresponding height of the lobes
for thickness = 0.007 inches

Thickness (in)	Radius of Beads(in)	Height (in)
0.007000	0.037100	0.428103
0.007000	0.037800	0.405274
0.007000	0.038500	0.382004
0.007000	0.039200	0.358295
0.007000	0.039900	0.334146
0.007000	0.040600	0.309557

Table 4.11: Variation of radius of beads and the corresponding height of the lobes
for thickness = 0.005 inches

Thickness (in)	Radius of beads (in)	Height (in)
0.005000	0.042000	0.346620
0.005000	0.043000	0.294213
0.005000	0.043500	0.267539
0.005000	0.044500	0.213247

Ten equal plies each having a thickness of one-tenth the wall thickness and 0° fiber orientation were used to model the rectangular lobes of the composite column as shown in Fig. 4.23.

The beads of the star with beads cross-section composite column were modeled using ten equal plies each having a thickness of (radius of beads/10) and 0° fiber orientation as shown in Fig. 4.24.

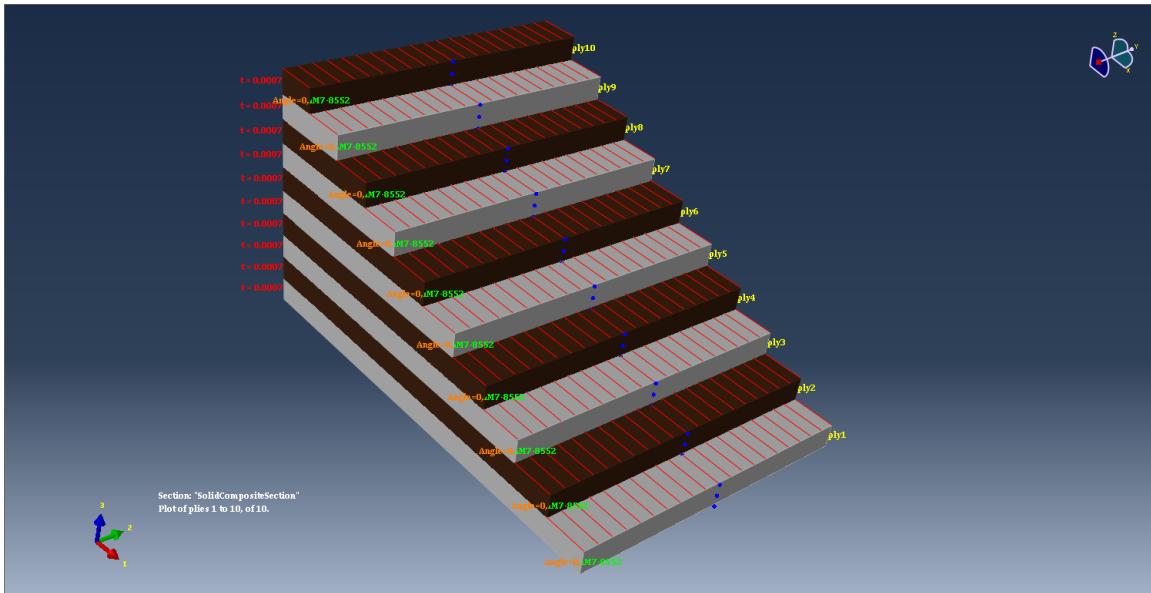


Figure 4.23 Ply stack plot for the rectangular lobes of star with beads cross-section composite column

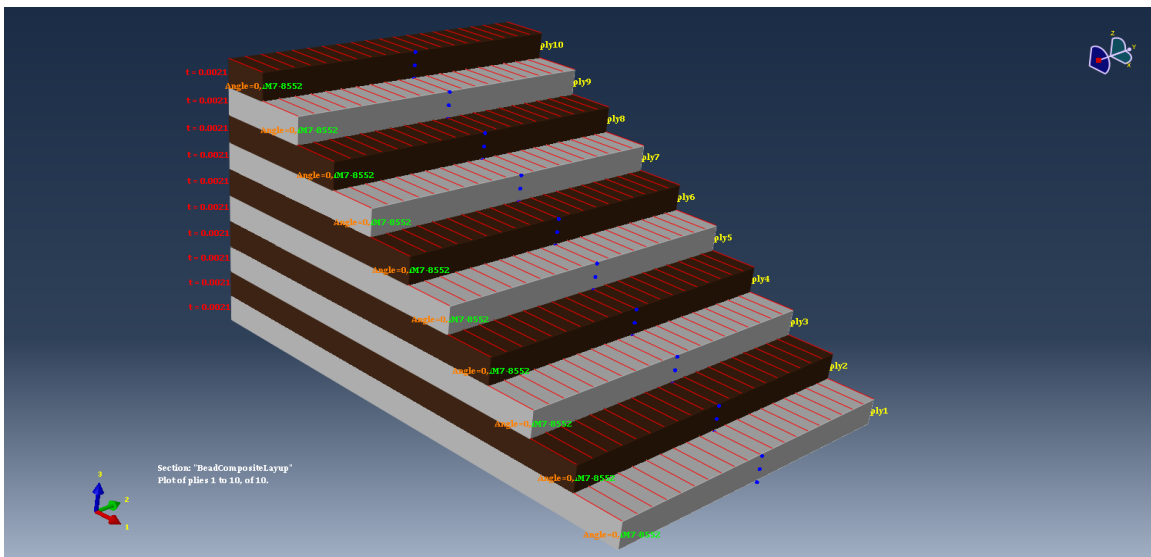


Figure 4.24 Ply stack plot for the beads of star with beads cross-section composite column

4.4.1 Meshing

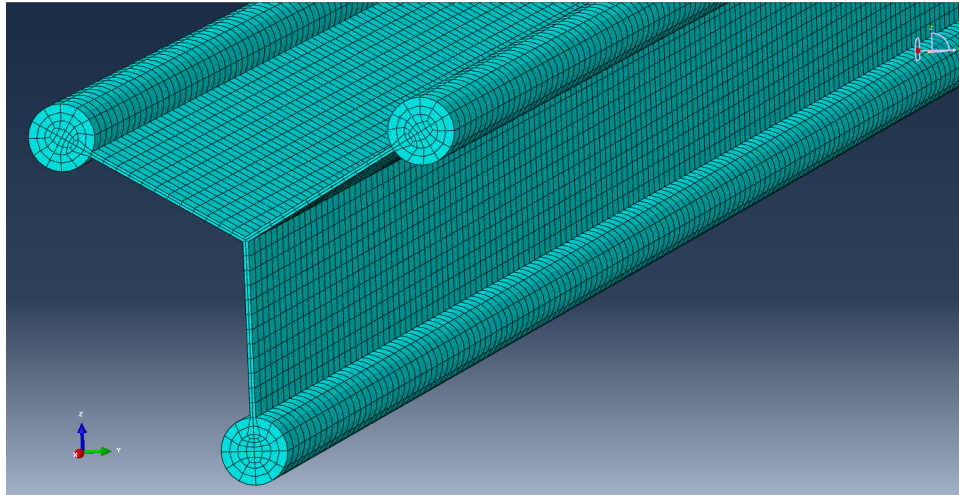


Figure 4.25 Mesh of C3D20R type star with beads cross-section composite column

The mesh of the star with beads cross-section composite column is shown in Fig.4.25. The maximum aspect ratio in the meshing of the star with beads cross-section composite column is 10.

4.4.2 Applied Load and Boundary Conditions

Pinned-pinned boundary conditions are imposed on star with beads cross-section composite column. The displacements along the x, y and z directions were constrained about the centroid as shown in Fig 4.26 to prevent the lateral displacement of the composite column.

The displacements along the y and z directions were constrained at both ends of the composite column as shown in Fig. 4.27 to effectively simulate the pinned-pinned boundary conditions.

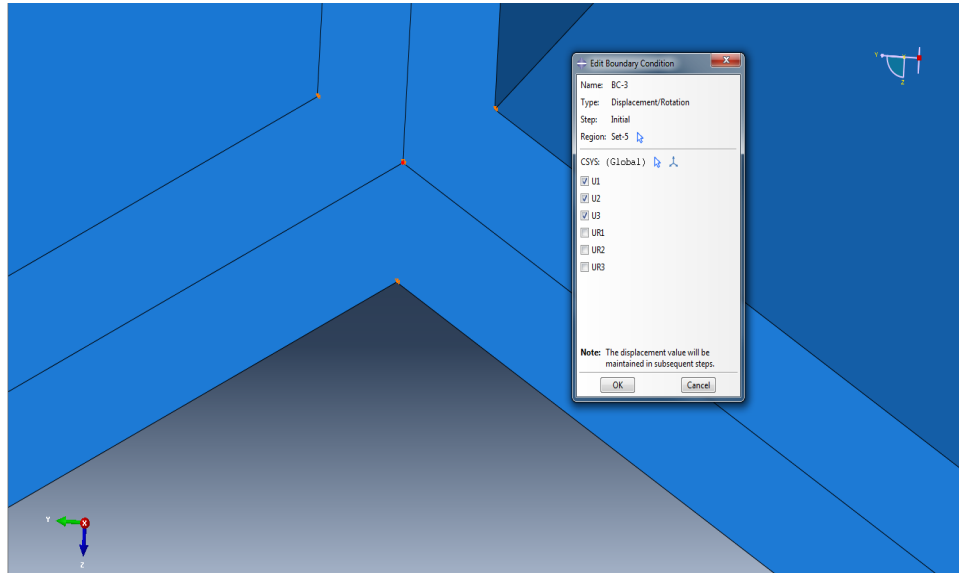


Figure 4.26 Constrain to prevent the lateral displacement of C3D20R type star with beads cross-section composite column

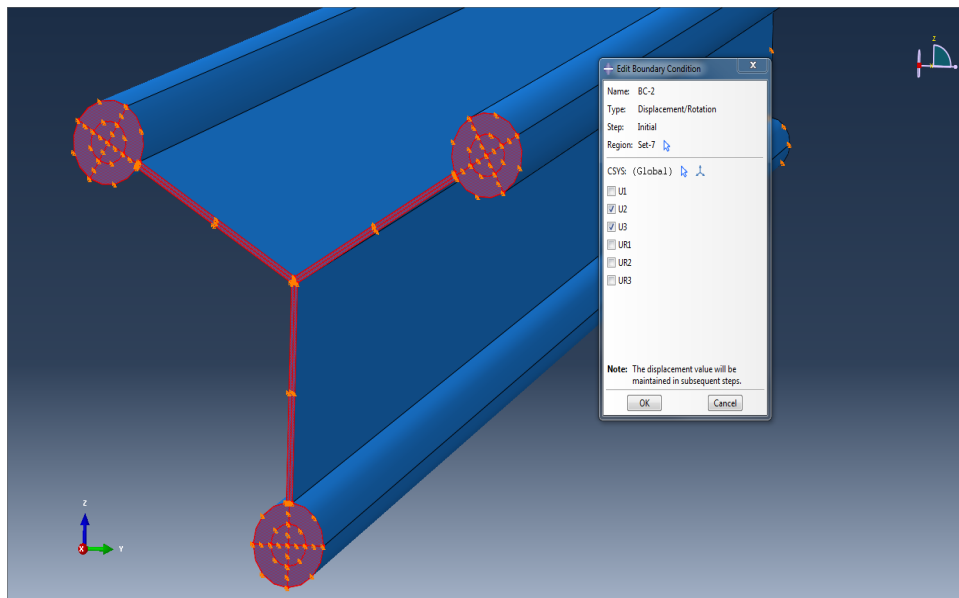


Figure 4.27 Constrains to simulate pinned-pinned boundary conditions for C3D20R type star with beads cross-section composite column

A uniform pressure of unit magnitude was applied at the top surface of the composite column as shown in Fig. 4.28, under the “Linear Perturbation, Buckle” analysis step to predict the buckling load for the star with beads cross-section composite column.

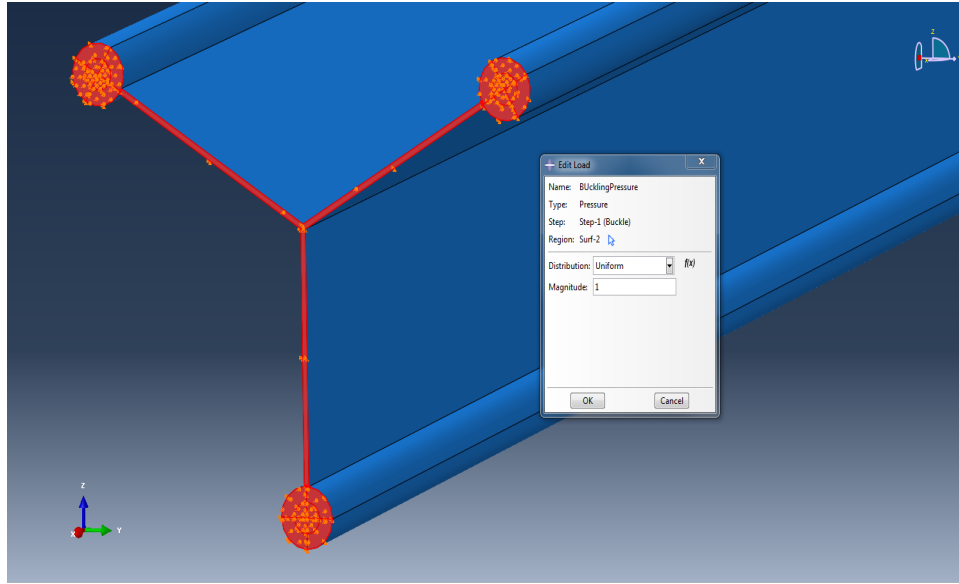


Figure 4.28 Uniform pressure for predicting the buckling load of star with beads cross-section composite column

CHAPTER 5






Results And Discussion

The relative area moment of inertia for regular polygonal cross-sections, normalizing the area moment of inertia of a circle is given in Table 5.1 and Fig. 5.1.

From Table 5.1 and Fig. 5.1 we can conclude that for a given cross-sectional area, the composite column with a solid equilateral triangular cross-section provides a higher buckling load than a solid circular cross section composite column.

Based on the above results, a tubular circular cross section composite column was compared with the tubular equilateral triangular cross section composite column to determine the optimum shape of the cross section.

Table 5.1 Relative area moments of inertia for regular polygonal cross-sections

Number of sides (n)	Shape of cross-section	Relative area moment of inertia I for constant area
3	Equilateral Triangle 	1.20920
4	Square 	1.04720
5	Regular Pentagon 	1.01697
6	Regular Hexagon 	1.00767
∞	Circle 	1.00000

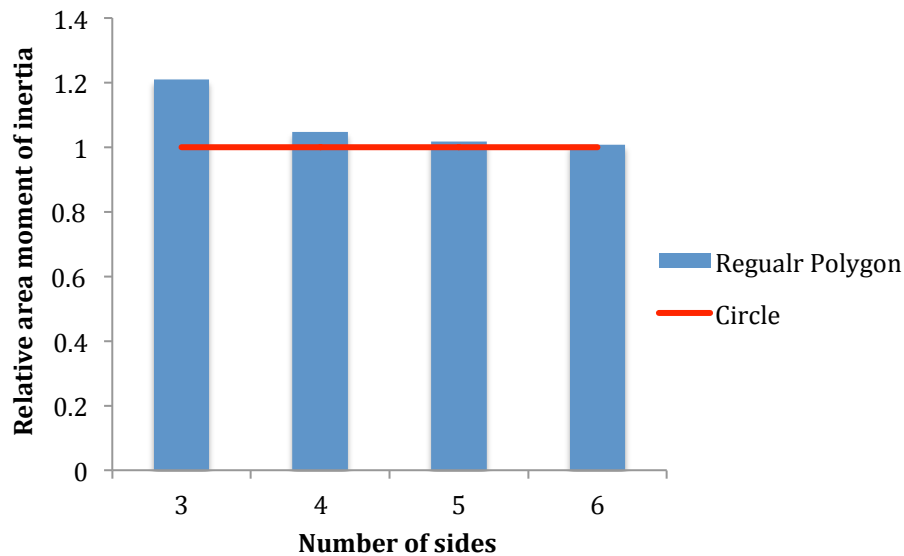


Figure 5.1 Relative area moments of inertia for regular polygonal cross-sections

The cross-sectional area moment of inertia should be increased so as to increase the buckling load of the composite column. This can be done without increasing the weight of the column by re-distributing the material as far from the principal axis of the cross section as possible, while keeping the material thick enough to prevent local buckling.

The transition between global and local buckling cannot be easily predicted using an analytical method, hence a finite element approach is used to determine the thickness for which the transition takes place. The transition point determines the maximum possible load that can be sustained for the cross section.

FEM does not distinguish between global and local buckling modes. Thus, it is the user who must classify the calculated modes, based on the deformed buckling mode shapes.

The deformed shape for the global buckling of composite column obtained using finite element analysis is as shown in Fig. 5.2.

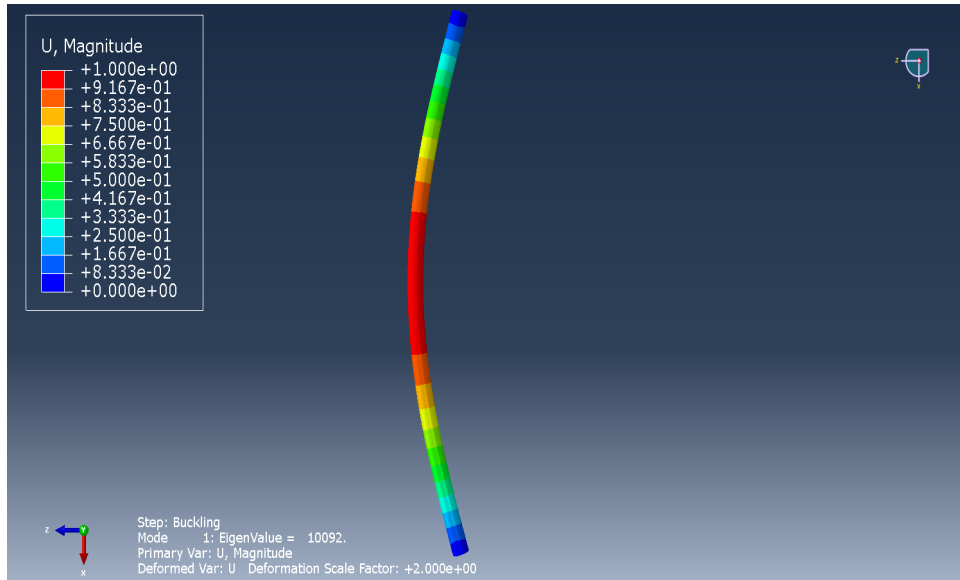


Figure 5.2 Deformed shape for the global buckling of composite column

5.1 Tubular Circular Cross-Section Composite Column

The critical loads obtained by using the S8R type shell elements for different values of thickness are given in Table 5.2.

The marked row indicates the transition from global to local buckling; it is characterized by a change in the mode of deformation and a drop in the critical load.

Beyond the point of transition as the thickness is further reduced, the buckling load reduces, which is not predicted by the Euler-Bernoulli's column buckling equation. Hence the difference between the analytical and finite element method predicted buckling load increases drastically.

Table 5.2 Critical loads for S8R type tubular circular cross-section composite columns

Thickness (in)	Shell Radius (in)	Critical Load Pcr(lb)	Analytical Pcr (lb)	%Error
0.0250	0.135000	64.4646	65.417	-1.45
0.0200	0.168750	100.051	101.702	-1.62
0.0150	0.225000	175.824	180.371	-2.52
0.0100	0.337500	383.760	405.473	-5.35
0.0093	0.362904	440.032	468.783	-6.13
0.0087	0.387932	498.458	535.652	-6.94
0.0084	0.401787	532.013	574.586	-7.41
0.0081	0.416668	568.970	617.927	-7.92
0.0078	0.432693	609.802	666.365	-8.49
0.0077	0.438313	599.849	683.783	-12.27
0.0076	0.44408	590.526	701.893	-15.87
0.0075	0.450000	572.697	720.1621	-20.48
0.0050	0.675000	289.866	1621.557	-82.12

The variation of critical load with respect to the thickness for C3D20R type tubular circular cross-section composite column is shown in Table 5.3

The study is carried out until the cross-section becomes a solid circle. As the thickness becomes large only C3D20R element type is used to predict the buckling load. Using both C3D20R and S8R element types the critical thickness for the tubular circular cross-section composite column is obtained to be 0.0078 in.

Table 5.3 Critical loads for C3D20R type tubular circular cross-section composite columns

Thickness (in)	Inner Radius (in)	Outer Radius (in)	Critical Load Pcr (lb)	Analytical Pcr (lb)	%Error
0.0820	0.000159	0.082159	11.9944	12.0114	-0.14
0.0810	0.001167	0.082167	11.9993	12.0162	-0.14
0.0800	0.002188	0.082188	12.0012	12.0284	-0.23
0.0750	0.007500	0.082500	12.1893	12.2115	-0.18
0.0700	0.013214	0.083214	12.3825	12.6328	-1.98
0.0650	0.019423	0.084423	13.2890	13.3540	-0.49
0.0600	0.026250	0.086250	14.3858	14.4637	-0.54
0.0550	0.033864	0.088864	16.0447	16.0925	-0.30
0.0500	0.042500	0.092500	18.3778	18.4397	-0.34
0.0450	0.052500	0.097500	21.7529	21.8206	-0.31
0.0400	0.064375	0.104375	26.6663	26.7600	-0.35
0.0350	0.078929	0.113929	34.0311	34.1825	-0.44
0.0300	0.097500	0.127500	45.5670	45.8434	-0.60
0.0250	0.122500	0.147500	64.8516	65.4175	-0.87
0.0200	0.158750	0.178750	100.331	101.702	-1.35
0.0150	0.217501	0.232501	176.099	180.371	-2.37
0.0100	0.332501	0.342501	384.631	405.473	-5.14
0.0093	0.358254	0.367554	441.187	468.783	-5.89
0.0087	0.383582	0.392282	499.990	535.652	-6.66
0.0084	0.397587	0.405987	533.771	574.586	-7.10
0.0081	0.412618	0.420718	571.030	617.927	-7.59
0.0078	0.428793	0.436593	612.233	666.365	-8.12
0.0077	0.434463	0.442163	603.666	683.783	-11.72
0.0076	0.440280	0.447880	589.564	701.893	-16.00
0.0075	0.446251	0.453751	575.971	720.732	-20.09
0.0050	0.672502	0.677502	278.856	1621.557	-82.80

As the thickness is reduced, near the points of transition, the assumptions of Euler-Bernoulli's column buckling equation do not hold true and S8R element type predicts the buckling load more accurately than the analytical solution.

Figure 5.3 shows the comparison of the critical load predicted by finite element method and analytical method as the thickness of the tubular circular cross-section is varied.

The peak of the finite element prediction displayed in the plot indicates the transition from global to local buckling and determines the maximum buckling load that can be sustained by the tubular circular cross-section composite column.

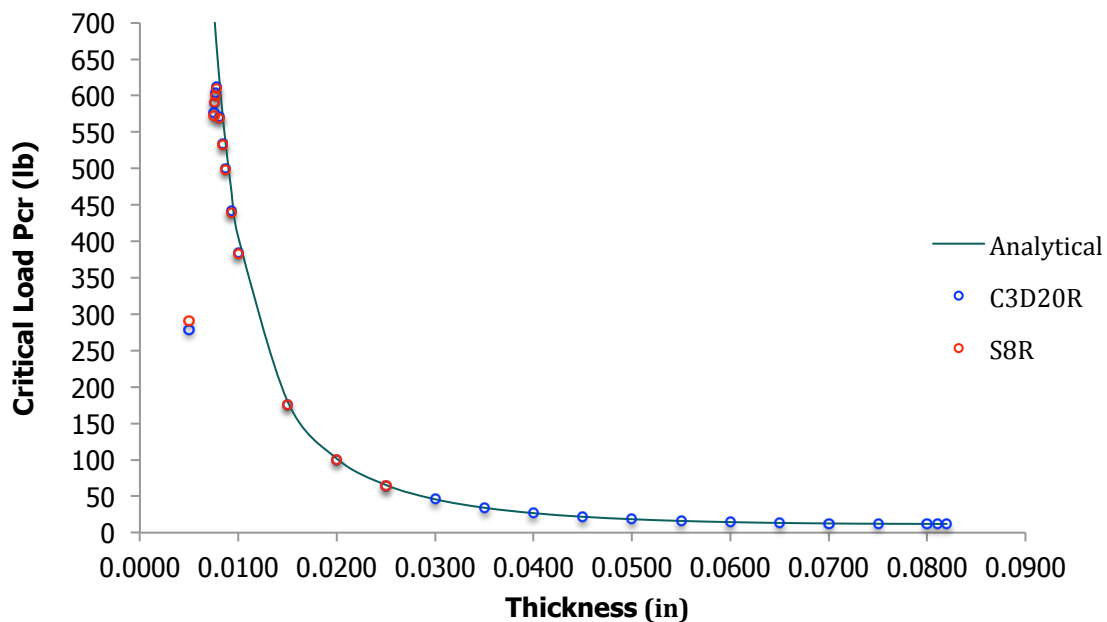


Figure 5.3 Plot of critical load vs. thickness for the tubular circular cross-section composite column

5.2 Tubular Equilateral Triangular Cross-Section Composite Column

The critical loads predicted using analytical and finite element method for different values of thickness are shown in Table 5.4.

The maximum critical load is obtained for a thickness of 0.0129 in and has a value of 172.952 lb.

Table 5.4 Critical load for tubular equilateral triangular cross-section composite column

Thickness (in)	Inner Side (in)	Outer Side (in)	Critical Load Pcr(lb)	Analytical Pcr (lb)	%Error
0.0638	0.000288	0.221298	14.5050	14.5242	-0.13
0.063	0.003081	0.221319	14.5105	14.5297	-0.13
0.0620	0.006623	0.221397	14.5309	14.5501	-0.13
0.0610	0.010224	0.221534	14.5667	14.5861	-0.13
0.0600	0.013887	0.221733	14.6189	14.6385	-0.13
0.0550	0.033257	0.223783	15.1581	15.1802	-0.15
0.0500	0.054769	0.227975	16.2761	16.3034	-0.17
0.045	0.079138	0.235022	18.2012	18.2389	-0.21
0.0400	0.107433	0.245997	21.3139	21.3702	-0.26
0.0350	0.141338	0.262582	26.2825	26.3732	-0.34
0.0300	0.183658	0.287582	34.3555	34.5314	-0.51
0.0250	0.239443	0.326045	48.1647	48.5311	-0.75
0.0200	0.318789	0.388071	78.1391	74.8039	4.46
0.0150	0.445259	0.497221	129.207	132.120	-2.20
0.0145	0.462375	0.512604	137.988	141.334	-2.37
0.0140	0.480651	0.529149	147.690	151.557	-2.55
0.0135	0.500217	0.546983	158.443	162.941	-2.76
0.0130	0.521222	0.566255	170.399	175.667	-3.00
0.0129	0.525610	0.570297	172.952	178.392	-3.05
0.0128	0.530064	0.574405	171.169	181.181	-5.53
0.0127	0.534586	0.578580	165.863	184.036	-9.87
0.0126	0.539176	0.582824	160.687	186.960	-14.05
0.0125	0.543837	0.587139	155.625	189.954	-18.07
0.0100	0.689539	0.724181	63.5305	296.547	-78.58

Figure 5.4 shows the variation of critical load with the thickness for the tubular equilateral triangular cross-section composite column.

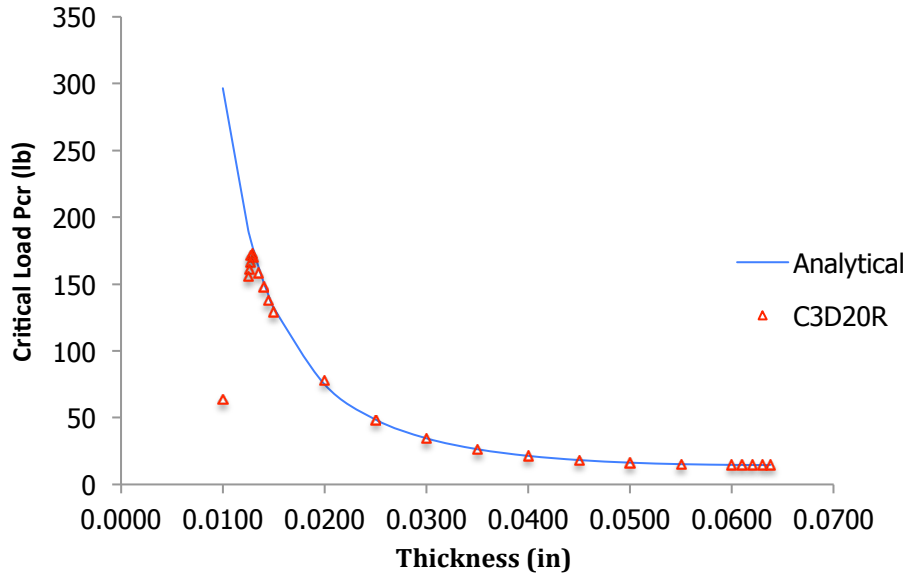


Figure 5.4 Plot of critical load vs. thickness for the tubular equilateral triangular cross-section composite column

5.3 Comparison of Maximum Critical Load for Tubular Circular and Tubular Equilateral Triangular Cross-Section Composite Columns

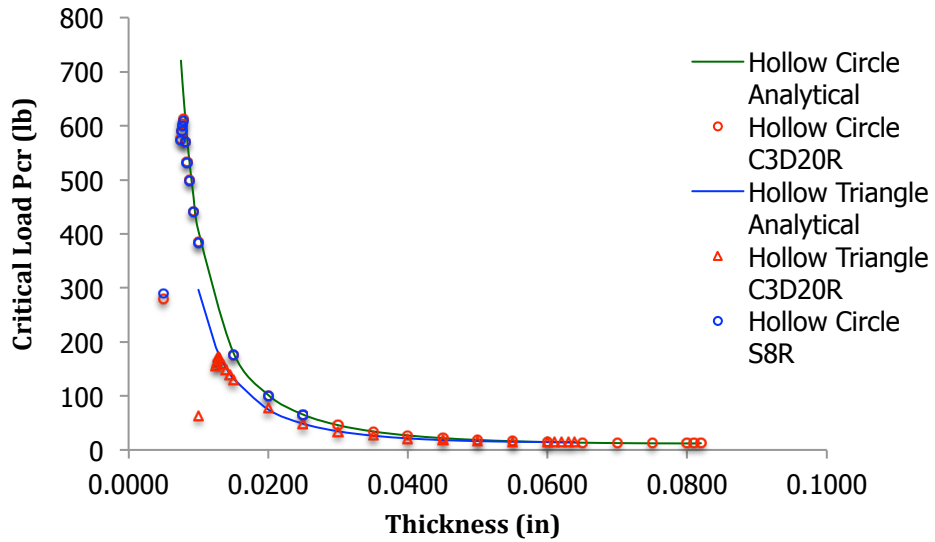


Figure 5.5 Plot of critical load vs. thickness for tubular circular and equilateral triangular cross section composite columns

Figure 5.5 gives a comparison of the critical load for the tubular circular and equilateral triangular cross-section composite columns. The maximum critical load for the tubular circular cross-section is 609.82 lb whereas that for the tubular equilateral triangular cross-section is 172.952 lb. Therefore; a tubular circular cross-section is better than a tubular equilateral triangular cross-section for the arrow shaft.

This result is counterintuitive, as we know that for solid cross-sections having the same area, an equilateral triangular cross-section provides a buckling load 20.92% higher than a solid circular cross-section.

To better understand these results, the thickness is increased until the tubular circular and tubular equilateral triangular cross-sections become solid cross-sections and the critical loads predicted are compared.

On closer inspection we find that the variation of thickness for the tubular circular and tubular equilateral triangular cross-sections do not follow the same path. The thickness for a tubular circular cross-section is given by $(r_2 - r_1)$, whereas thickness for a tubular equilateral triangular cross-section is given by $\frac{(b_2 - b_1)}{2\sqrt{3}}$. The value of the thickness for which the tubular equilateral triangle becomes a solid cross-section is $t = 0.063883$ inches, whereas a tubular circular cross-section becomes a solid circle for thickness $t = 0.082158$ inches. Thus as the thickness is increased the tubular triangular cross-section becomes a solid triangular cross-section but for the same value of thickness, the tubular circular cross-section has not converged to a solid circle. Figure 5.6 shows that a tubular triangular cross-section converges into a solid cross-section faster than the tubular circular cross-section due to which the critical load for the solid equilateral triangular cross-section is 20.92% higher than that for a solid circle.

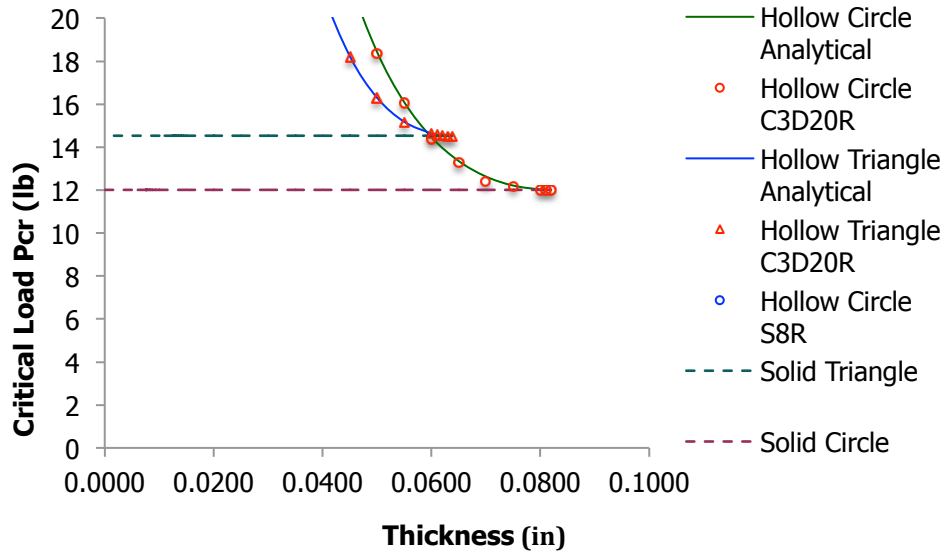


Figure 5.6 Comparison of the critical load vs. thickness for solid and tubular circular and equilateral triangular cross-section columns

5.4 Star Shaped Cross-Section Composite Column

The variation of the critical load for the star shaped cross-section composite column with the thickness is shown in Table 5.5. The maximum critical load is obtained for a thickness of 0.016 inches and has a value of 234.7428 lb. Figure 5.7 shows the plot of critical load vs. thickness for the star shaped cross-section composite column

Table 5.5 Critical load for star shaped cross-section composite column

Thickness (in)	Height (in)	Critical Load Pcr (lb)	Analytical Pcr (lb)	%Error
0.221298	0.000000	14.5092	14.524	-0.10
0.220000	0.000376	14.5205	14.523	-0.02
0.200000	0.006475	14.2851	14.289	-0.03
0.150000	0.025473	12.8132	12.818	-0.04
0.100000	0.056252	12.9067	12.912	-0.04
0.050000	0.134155	28.2440	28.245	0.00
0.040000	0.170941	41.2559	41.261	-0.01
0.030000	0.231290	69.7968	69.822	-0.04
0.020000	0.350543	151.7869	151.963	-0.12
0.019000	0.369289	167.7315	167.958	-0.13
0.018000	0.390102	186.4032	186.694	-0.16
0.017000	0.413346	208.4488	208.837	-0.19
0.016000	0.439478	234.7482	235.264	-0.22
0.015000	0.469075	186.2802	267.153	-30.27
0.010000	0.705417	37.1674	596.405	-93.77
0.005000	1.412998	2.3770	2374.589	-99.90

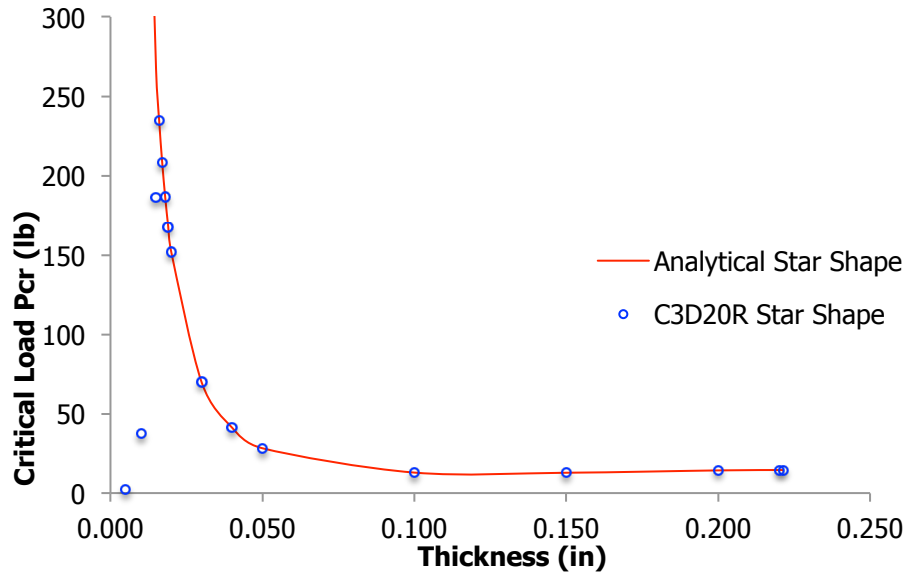


Figure 5.7 Plot of critical load vs. thickness for the star shaped cross-section composite column

5.5 Comparison of the Maximum Critical Load for the Star Shaped Cross-Section with Tubular Circular and Equilateral Triangular Cross-Section Composite Columns

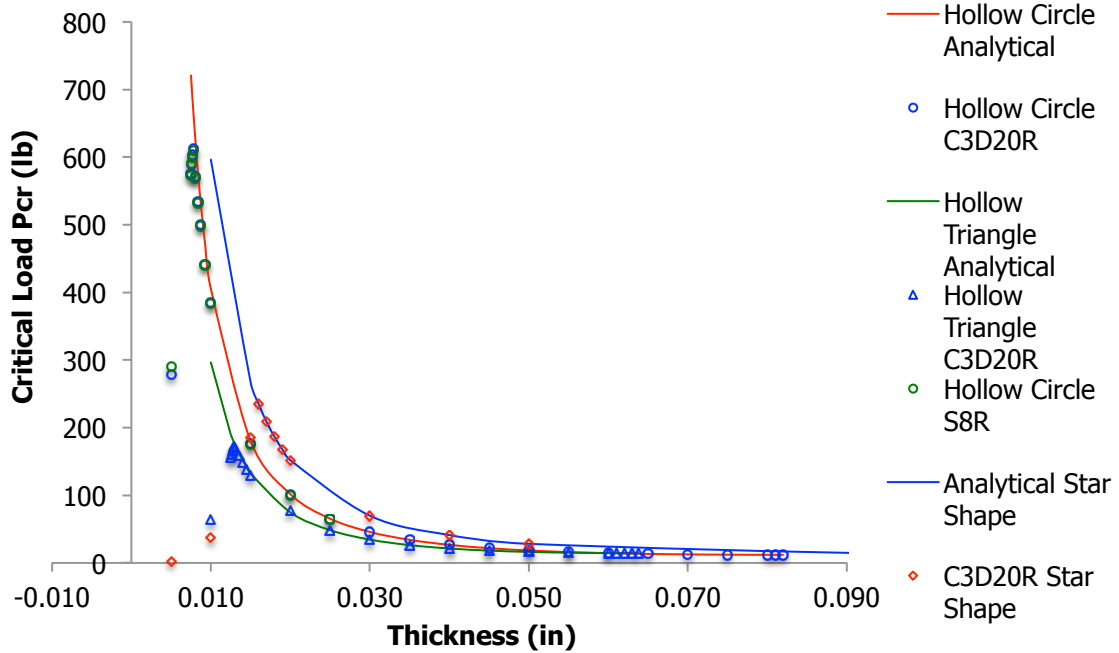


Figure 5.8 Plot of critical load vs. thickness for tubular equilateral triangular, tubular circular and star shaped cross-section composite columns

Figure 5.8 shows the variation of the critical load with wall thickness for the tubular circular, tubular equilateral triangular and star shaped cross-section composite columns. The maximum critical load for the star shaped cross-section composite column is 234.7482 lb, whereas that for the tubular circular and tubular equilateral triangular cross-section composite columns are 609.802 lb and 172.952 lb respectively. Hence the star shaped cross-section is better than the tubular equilateral triangular cross-section. However, the optimum cross-section among these three is the tubular circular cross-section.

5.6 Star With Beads Cross-Section Composite Column

For the star shaped cross-section composite column, the transition between local and global buckling takes place at thickness = 0.016 in. For a thickness ≥ 0.016 inches, irrespective of the radius of the beads, the star with beads cross-section will have a lower area moment of inertia and hence a lower buckling load than the star shaped cross-section without beads, as the area is distributed near the centroid in case of the star with beads cross-section. Hence the values of thicknesses < 0.016 inches are considered for analyzing the star with beads cross-section composite column.

For different values of thickness, the radius of the beads is increased and the transition from local to global buckling is determined as shown in Tables 5.6 – 5.12

Table 5.6 Variation of the critical load with the radius of the beads for
thickness = 0.015 in

Thickness (in)	Radius of Bead (in)	Height (in)	Pcr (lb)
0.015000	0.015000	0.436300	204.5003
0.015000	0.018000	0.418681	232.6276
0.015000	0.019500	0.408444	255.6783
0.015000	0.022500	0.385122	245.9237
0.015000	0.030000	0.310264	199.3791
0.015000	0.045000	0.089751	31.88080

Table 5.7 Variation of the critical load with the radius of the bead for
thickness = 0.011 in

Thickness (in)	Radius of beads(in)	Height (in)	Critical Load Pcr(lb)
0.011000	0.029700	0.418617	338.2113
0.011000	0.030800	0.400717	339.4412
0.011000	0.031900	0.382125	319.5714
0.011000	0.033000	0.362841	298.4292
0.011000	0.034100	0.342866	276.1207

Table 5.8 Variation of the critical load with the radius of the beads for
thickness = 0.010 in

Thickness (in)	Radius of beads (in)	Height (in)	Critical Load Pcr(lb)
0.010000	0.027000	0.503239	188.3330
0.010000	0.030000	0.452534	270.9465
0.010000	0.031000	0.434375	305.7876
0.010000	0.033000	0.396170	354.8367
0.010000	0.034000	0.376126	330.3440
0.010000	0.040000	0.242657	168.6010

Table 5.9 Variation of the critical load with the radius of the beads for
thickness = 0.009 in

Thickness (in)	Radius of beads (in)	Height (in)	Critical Load Pcr(lb)
0.009000	0.033300	0.449961	270.4800
0.009000	0.034200	0.430224	303.3066
0.009000	0.034200	0.409921	341.4134
0.009000	0.035100	0.389052	364.8246
0.009000	0.036000	0.367618	335.6242
0.009000	0.036900	0.345618	305.7452
0.009000	0.037800	0.323052	275.3785

Table 5.10 Variation of the critical load with the radius of the beads for
thickness = 0.008 in

Thickness (in)	Radius of beads (in)	Height (in)	Critical Load Pcr(lb)
0.008000	0.035200	0.430975	279.7681
0.008000	0.036000	0.409408	314.0791
0.008000	0.036800	0.387339	354.7942
0.008000	0.037600	0.364767	380.8986
0.008000	0.038400	0.341692	312.7219
0.008000	0.039200	0.318115	278.7502
0.008000	0.040000	0.294035	245.0118

Table 5.11 Variation of the critical load with the radius of the beads for
thickness = 0.007 in

Thickness (in)	Radius of beads (in)	Height (in)	Critical Load Pcr(lb)
0.007000	0.037100	0.428103	252.9852
0.007000	0.037800	0.405274	283.9033
0.007000	0.038500	0.382004	320.6529
0.007000	0.039200	0.358295	350.4046
0.007000	0.039900	0.334146	312.7219
0.007000	0.040600	0.309557	275.4209

Table 5.12 Variation of the critical load with the radius of the beads for
thickness = 0.005 in

Thickness (in)	Radius of beads (in)	Height (in)	Critical Load Pcr(lb)
0.005000	0.042000	0.346620	175.8618
0.005000	0.043000	0.294213	207.8423
0.005000	0.043500	0.267539	225.3752
0.005000	0.044500	0.213247	150.1519

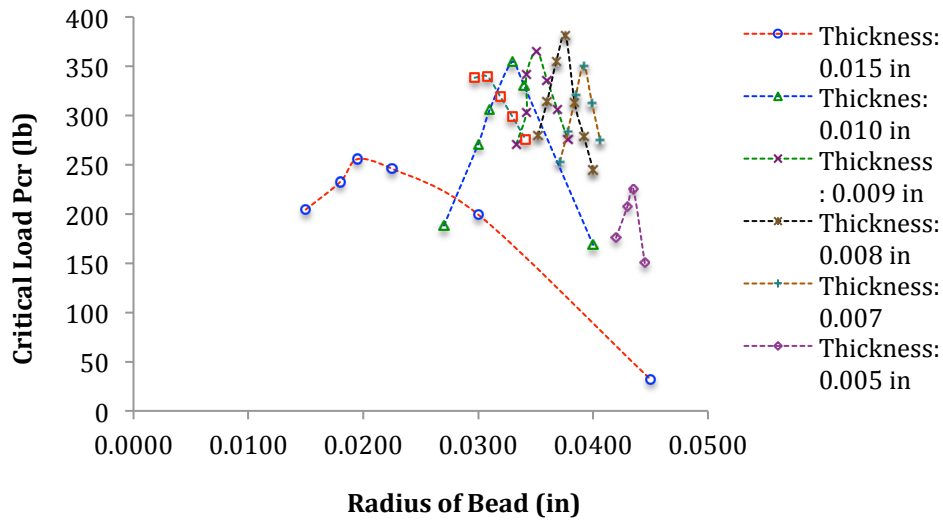


Figure 5.9 Variation of critical load with radius of beads for star with beads cross-section composite column

Figure 5.9 shows the variation of critical load with respect the radius of the beads for different values of thicknesses.

From Fig. 5.9, we can see that the peak of the curve that marks the maximum critical load increases with the reduction in thickness from 0.015 inches to 0.008 inches and decreases as the thickness is reduced below 0.008 inches.

The maximum value of the critical load for the different thicknesses and the corresponding bead radius is shown in Table 5.13.

A plot of the maximum critical load vs. the thickness for the star with beads cross-section composite column is shown in Fig. 5.10.

Table 5.13 Maximum critical load for different thickness of star with bead cross-section composite column

Thickness (in)	Radius of beads (in)	Height (in)	Maximum Pcr (lb)
0.015	0.019500	0.408444	255.6783
0.011	0.030800	0.400717	339.4412
0.010	0.033000	0.396170	354.8367
0.009	0.035100	0.389052	364.8246
0.008	0.037600	0.364767	380.8986
0.007	0.039200	0.358295	350.4046
0.005	0.043500	0.267539	225.3752

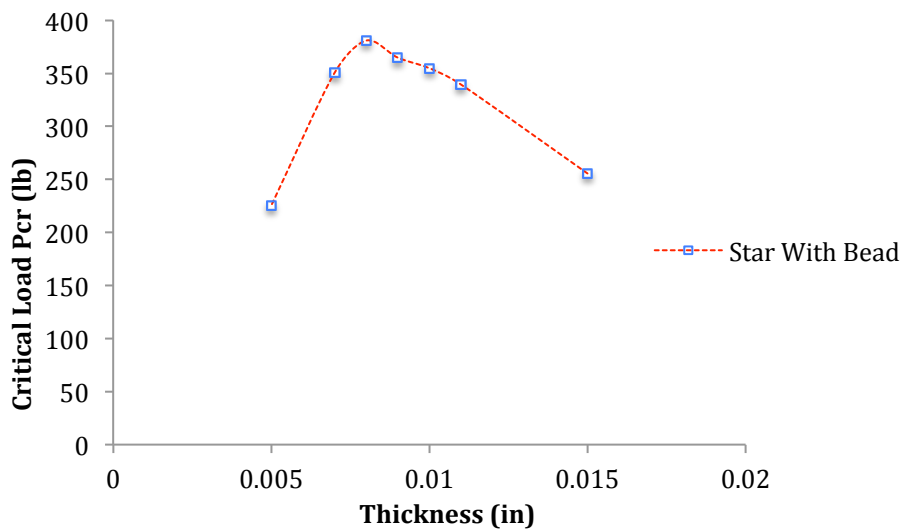


Figure 5.10 Plot of maximum critical load vs. thickness for the star with beads cross section composite column

From Table 5.13 and Fig. 5.10 we can find that the critical load corresponding to the thickness of 0.008 inches is the highest and has a value of 380.8986 lb.

Thus the dimensions of the star with beads cross section for which we get the highest critical load are thickness = 0.008 inches and radius of beads = 0.0376 inches.

5.7 Comparison of Maximum Critical Load for all the Cross-Sections

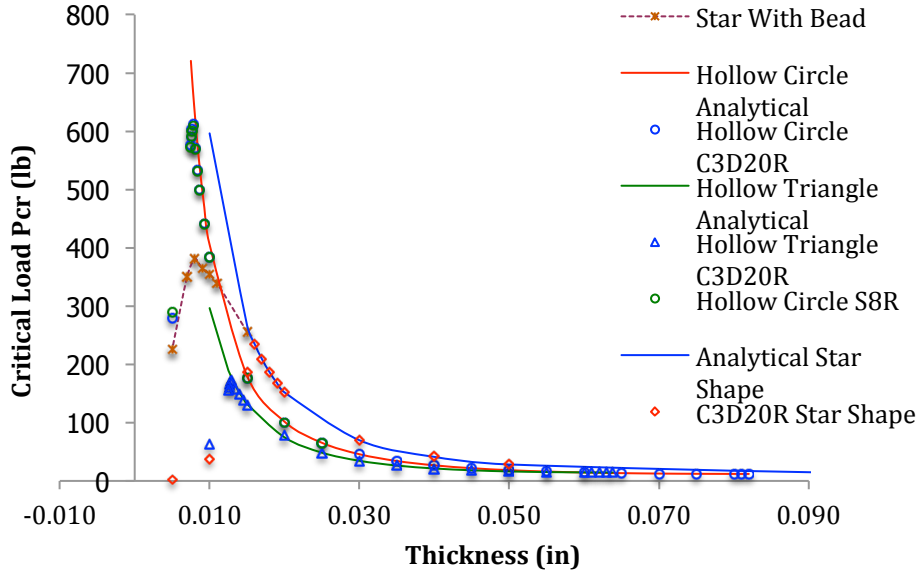


Figure 5.11 Plot of the critical load vs. thickness for all cross-sectional shapes

The plot of the variation of critical load with the wall thickness for all the cross-sectional shapes is shown in Fig. 5.11

From Fig. 5.11, we can see that the tubular circular cross-section composite column has the highest peak and hence provides the highest critical load of 609.802 lb. The star with beads cross-section is better than the star cross-section, which is better than the tubular equilateral triangular cross-section composite column.

CHAPTER 6

Conclusions And Recommendations

6.1 Conclusions

From the results obtained by analyzing the four cross-sections we can conclude that the tubular circular cross-section provides the highest buckling load. Thus among the four cross-sectional shapes considered, the tubular circular cross-section is the optimum shape for the composite arrow shaft.

6.2 Recommendations for Future Work

In this study, the area of the cross-section was considered to be uniform along the length of the column. A study with a varying cross-sectional area at constant arrow volume can be performed.

The orientation of the fibers is considered to be only along the length of the column. A study to find the optimum composite layup for practical layups must be undertaken.

In this study only 4 cross-sectional shapes were analyzed. Other cross-sectional shapes can be considered and the optimum can be determined.

References

- [1] Kooi, B.W., " Bow-Arrow Interaction in Archery," *Journal of Sports Sciences*, vol. 16, no. 8, pp. 721-731, 1998.
- [2] Kooi, B.W. and Sparenberg, J.A., " On the Mechanics of the Arrow," *Journal of Engineering Mathematics*, vol. 31, no. 2, pp. 285-306, 1997.
- [3] Rieckman, M., Codrington, J., and Cazzolato, B., "Modelling the Vibrational Behavior of Composite Archery Arrows," *Proceedings of the Annual Conference on the Australian Acoustical Society (Acoustics 2011), held on the Gold Coast, Australia, D. Mee and I. Hillock (eds.):* pp. 1-8, 2011.
- [4] Rieckmann, M., Park, J.L., Codrington, J., and Cazzolato, B., "Modelling the Three-Dimensional Vibration of Composite Archery Arrows under Free-Free Boundary Conditions," *Proceedings of the institution of Mechanical Engineers, Part P: Journal of Sports Engineering and Technology*, vol. 226, no. 2, pp. 114 - 122, 2012.
- [5] Lekavich, C. W., "Arrow Shaft," US Patent 5,273,293, December 28, 1993.
- [6] Becker, P. R., " Fluted Arrow," US Patent 6,595,880, July 22, 2003.
- [7] Asherman, R., " Arrow Shaft," US Patent 8,915,806, December 23, 2014.
- [8] Gere, J. M., Goodno, B. J., "Mechanics of Materials," *Cengage Learning, Eighth Edition*, pp. 1036, 2013.
- [9] ABAQUS v6.14 Reference Manual.

Biographical Information

Anirudh Srinivas earned a B.E. Mechanical Engineering degree from Don Bosco Institute of Technology, Bangalore affiliated to Visvesvaraya Technological University, Belagavi, India in May 2014. Subsequently he joined the graduate program at the University of Texas at Arlington in August 2014 and started working under the guidance of Dr. D. S. Dancila from January 2015, graduating with a Master of Science in Mechanical Engineering degree in May 2016.